A Study on Ship Collision and Grounding Using Nonlinear Finite Element Method

by

Ainian Zhang

Submitted to the Department of Human and Engineered Environmental Studies

in partial fulfillment of the requirements for the degree of

Doctor of Philosophy

at the

University of Tokyo

February 2007

Acknowledgment

This study has been carried out under the supervision of Associate Professor Katsuyuki Suzuki. His insight, guidance and advice are greatly acknowledged. This research would not have been if not for him.

Professor Tetsuo Yuhara, Professor Toshiaki Hisata, Professor Yutaka Toi and Professor Hiroyuki Yamato have given useful advises. Their kindness are greatly appreciated.

Special thanks are given to Mr. Hisayoshi Endo at National Maritime Research Institute and Dr. Ge Wang at ABS. Their valuable discussions helped some aspects of the study.

I could not have pursued my research without the financial support of Monbusho and this support is greatly acknowledged.

Thanks for the friendly, exciting and dynamic work environment provided by our Laboratory. Thanks to Dr. Junji Sawamura. Mr. Jiro Yoshida, Dr. Syogo Nakasumi, for their sincere help. Thanks to fellow students for all their help and inspiration. Thanks for all the help extended to me by Jiangshui Shi, Kirkayak Leventand, De Souza Vinicius Aguiar and Ming Gao at various times.

Finally, I thank my wife Li Jing, my daughter Yangyang and my parents for their love, patience, encouragement and active supports throughout the research.

Contents

List of Figures

Chapter 1 Introduction

Chapter 2 An Overview of the Mechanics of Ship Collision and Grounding

Chapter 3 Numerical Analysis of Simple Component Failure Mode Axial Crushing of Thin-Walled Structure

Chapter 4 Numerical Simulation of Large Scale Bottom Structure Grounding Experiment

Chapter 5 Numerical Simulation of Fluid-structure Interaction of Liquid-filled Cargo Tank during Ship Collision

Chapter 6 A New Rational Numerical Simulation Procedure for Liquid Cargo Ship Collision

Chapter 7 Numerical Analysis Examples for Full Scale Liquid Cargo Ship Collision

Chapter 8 A New Simplified Analytical Internal Mechanics Model for Ship Side Structure Damage

Appendix

List of Tables

Chapter 7 Numerical Analysis Examples for Full Scale Liquid Cargo Ship Collision

Chapter 8 A New Simplified Analytical Internal Mechanics Model for Ship Side Structure Damage

Chapter 1 Introduction

1.1 Overview and Background

Ship collision and grounding have always been among the most hazardous accidents for floating structures, even if great effort is made to prevent them. According to world casualty statistics (LR 2000), Fig.1.1 illustrates the percentage of various type losses of ships during 1995-1998. Collision, contact and grounding (wrecked/stranded) account for 39% of total losses. The European project HARDER has established a damage database. Fig.1.2 shows the correlations between the striking ship length and the struck ship length and the correlations between the striking ship speed and struck ship speed. It is seen that the correlations are quite scattered.

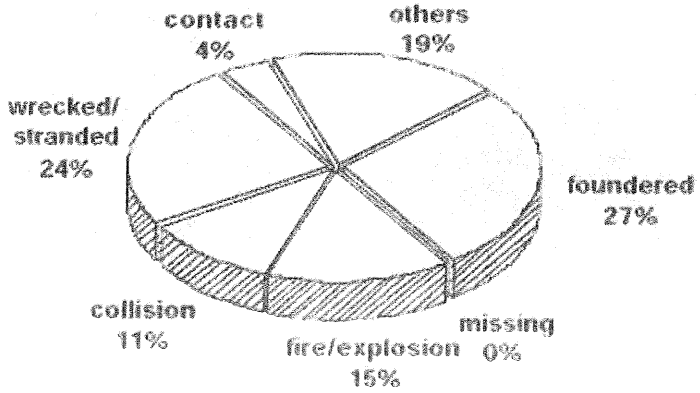

Fig. 1.1 Total loss causes for all types of ships during the years 1995-1998

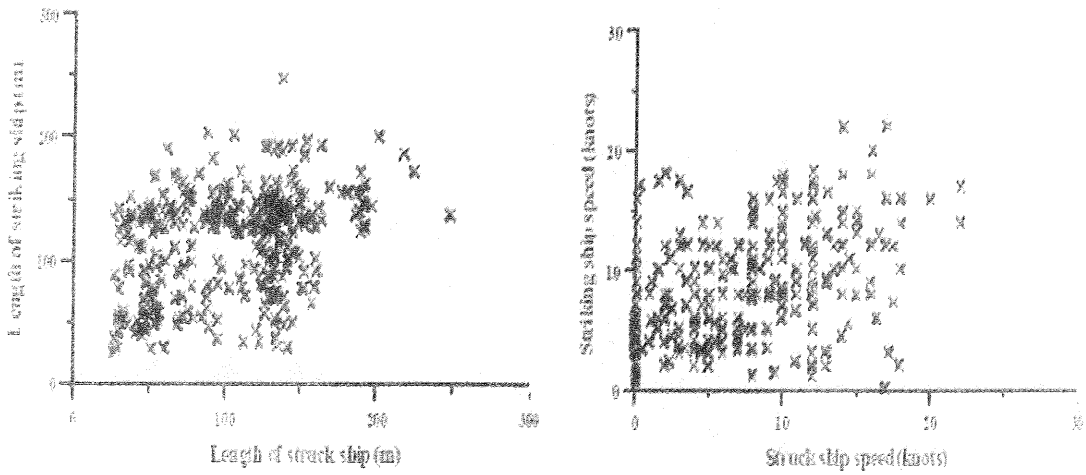

Fig. 1.2 HARDER damage database

Several serious collisions have resulted in a large number of lives lost and caused severe damage to the ecology of the accident areas. Fig.1.3 shows the damage in the ship collision accident, in which a 100,000 tonne single hull tanker was struck by a 23,000 tonne container ship in 1992. Consequently, 10,000 tonne oil was spilt and a fire disaster followed. Fig.1.4 shows a grounding accident, in which a 147,000 tonne tanker was grounded at Millford Haven harbor in UK. About 65,000 tonne of crude oil was split to the sea.

Fig. 1.3 Ship collision accident

Fig. 1.4 Ship grounding accident

With the increasing demand for safety at sea and for protection of the environment, it is of crucial importance to be able to reduce the probability of accidents, assess their consequences and ultimately minimize or prevent potential damages to the ships and the marine environment. International Maritime Organization (IMO) has taken many measures to minimize the oil outflow.

To solve the ship collision and grounding problem, at least two major tasks should be studied. One is to derive the probability distribution from various collision and grounding scenarios in a given area. The other is to predict the ship responses in a collision or grounding. Since early 1990s, many predictive calculation procedures have been developed to predict the ship responses in a collision or grounding. These methods have matured to such a level that they are now being integrated into systems for evaluation and designs. Nevertheless, how to calculate the ship responses in an accident continues to stand in the center of most of the recent research and development.

1.2 Objective of the Work

For liquid products tanker carrying hazardous cargo (such as crude oil), damage is not acceptable if it results in cargo outflow with disastrous consequences to environment. A major challenge in liquid products ship collision and grounding analysis is the prediction of the structure damage and the energy dissipation correctly where the fluid-structure interactions of liquid products in tank and surrounding water are taken into account.

The Arbitrary Langrangian Eulerian (ALE) finite element method solves the transient equations of motion of the fluid and structure using the explicit time integration method. Fluid/structure coupling calculations are carried out each time step. This method is suitable to analyze highly dynamic, highly nonlinear phenomena lasting for short time such as the interaction of the liquid cargo in tank and surrounding water during ship collision.

The main objective of this thesis is to improve the existing methods on numerical simulation of oil tanker collision and grounding by considering the effect of liquid cargo in tank and surrounding water using ALE FE method.

To evaluate fluid-structure interaction of liquid cargo filled tank during ship collision and grounding, four different numerical models will be adopted to model fluid-structure

interaction in liquid filled cargo tank, namely Arbitrary Lagrangian Eulerian model, Lagrangian FE model, Linear Sloshing model and Rigid Point Mass model.

Using ALE FE method, a rational procedure for assessing the crashworthiness of liquid products tanker structures, where the effect of liquid cargo in tank and surrounding water is taken into account, will be proposed.

Since ALE FE method requires enormous modeling efforts and computing time, it is necessary to establish a reliable and practical assessment procedure for structural response and estimating oil outflow in side collision. Considering the dynamic effect during ship side collision, the new simplified analytical model for impact force is proposed. Application of new simplified method, estimation of the mean oil outflow in probabilistic analysis is carried out.

1.3 Organization of Chapters

This dissertation consists of eight chapters.

In Chapter 2 an overview of the previous researches on the external dynamics and the internal mechanics in ship collision and grounding is presented. The motion equations and the hydrodynamic coefficients in frequency domain and time domain are introduced. Four analysis methods of internal mechanics, namely Empirical formulae, Simplified analytical approach, Simplified FEM and Nonlinear FEM simulation, are discussed. The advantage and disadvantage of each method are summarized.

In Chapter 3 benchmark studies on simplified analytical methods, nonlinear FEM and experimental results for axial crushing of thin-walled structure are performed. Based on the experimental data, the new equivalent plate thickness and mean crushing load formulas for the stiffened tubes are derived. As the application example, the proposed new ultimate load and mean crushing load formulas are checked by the structural response of bow crushing test.

In Chapter 4 benchmark studies on nonlinear FEM and experimental results for the single-hull bottom structure are performed. The effect of selected parameters on crashworthiness of the single-hull bottom structure due to raking is studied by nonlinear FE method. Several practical ways to improve computing efficiency, accuracy and stability for

ship grounding experiment simulation are given and some guidelines for nonlinear FEM analyses are proposed.

In Chapter 5 the ALE finite element method is validated by the rectangular sloshing experiment. Four different numerical FE models for liquid cargo in tank were used to analyse ship collision between a 72,000 tonne tanker and the crude oil tanker of a 293,000 tonne double hull VLCC. The structural responses, damage extent and energy dissipations for different models are compared.

In Chapter 6 numerical simulation of the ship collision taking account of both fluid-structure interaction in liquid cargo tank and surrounding water is presented. Two different numerical FE models for surrounding water were used to analyze ship collision between 350,000 tonne VLCC and 293,000 tonne double hull VLCC. A new rational procedure for assessing the crashworthiness of liquid products tanker structures, where the effect of liquid cargo in tank and surrounding water is taken into account, is proposed.

In Chapter 7 a serial of numerical analysis of full-scale ship collision are performed in order to understand the structural damage behavior and energy dissipation deeply. The detailed parameter study is carried out. The effect of the following parameters such as collision angle, the striking ship velocity, struck ship velocity and the striking ship mass is discussed.

In Chapter 8 a simplified practical design oriented procedure for the side structural response analysis is presented. Numerical examples of ship-ship collisions in different collision conditions are performed. This new simplified analytical method is incorporated into a probability-based framework to properly assess structural performance and estimate the mean oil outflow for a variety of damage scenarios.

Chapter 9 summarizes all these studies, and gives suggestions for further researches.

Chapter 2 An Overview of the Mechanics of Ship Collision and Grounding

2.1 Introduction

This chapter provides an overview of research achievements of the past and current, which focus on the mechanics of collision and grounding events. The analysis of the accident mechanics can be divided into two parts; namely the internal mechanics and the external mechanics. Although those two parts are studied separately, they are linked together with the common contact force. The external mechanics deals with the rigid body global motion of the ships under the action of the collision or grounding force and the hydrodynamic pressures acting on the wet surface. The internal mechanics includes evaluation of the structural failure response of the involved ships during collision and grounding.

2.2 External Mechanics

The hydrodynamic effect of the surrounding water should be taken into account in dealing with the absorbed energy during collision between two ships. In many cases (notably collisions) the motion of the struck ship during the contact phase is small, and the inertia force is the most important contribution. Minorsky (1959), in his famous paper, assumed that the hydrodynamic effect was represented by an increased inertia force due to added mass effect and estimated the added mass coefficient of the struck ship to be 0.4 (added mass coefficient for lateral vibration). In fact, the hydrodynamic force in a transient condition such as collision is a function of time as well acceleration. In 1982, Petersen studied the procedure for time simulation of the external dynamics in ship collisions. The hydrodynamic forces acting on the ship's hull during the collision were calculated by a strip theory. The involved ships were treated as essentially stiff bodies with all deformations taking place in the contact area. The structural response in the contact area was modeled as nonlinear springs. Based on rigid-body motion theory and strip theory (Pedersen 1995, Pedersen and Zhang 2000, Brown 2002, Paik et al. 1999, Nolau Neto et al. 2004, Suzuki et al. 2000, 2001, Reich and Roher 2004), simplified methodologies for external mechanics were often used.

2.2.1 Equations of Motion for a Ship

To describe the motion of ship in wave, the right –handed co-ordinate system is defined in Fig. 2.1. The origin is fixed to the ships' centre of gravity. The transverse displacements along x, y and z axes are denoted by surging (x_1), swaying (x_2) and heaving (x_3) respectively. The angular displacements of the rotational motion along x, y and z axes are denoted by rolling (x_4), pitching (x_5) and yawing (x_6) respectively. Suppose that the ship oscillates as a rigid body in six degrees of freedom with amplitudes of x_i ($i = 1,2\ldots6$). Here i=1, 2, 3, 4, 5 and 6 refer to surge, sway, heave, roll, pitch, and yaw respectively.

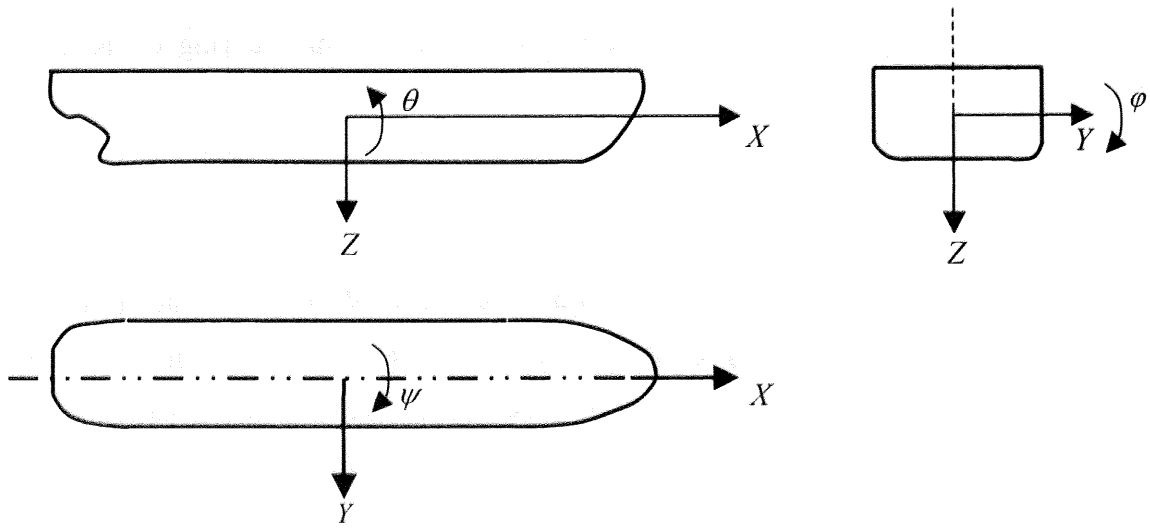

Fig. 2.1 The local coordinate system with origin at the centre of gravity

Under the assumption that the loads acting on a floating struck ship consist of hydrostatic restoring forces expressed in terms of spring and hydrodynamic forces expressed in terms of added mass and damping, the general formulation of equations of motion can be written in the following form:

$$\sum_{k=1}^{6}\left[\left(M_{j,k}+A_{j,k}\right)\cdot\ddot{x}_k+B_{j,k}\cdot\dot{x}_k+C_{j,k}\cdot x_k\right]=F_j \qquad j=1\ldots6 \qquad (2.1)$$

where

$M_{j,k}$ the components of the generalized mass matrix for the ship

$A_{j,k}$ and $B_{j,k}$ the add-mass and damping coefficients

$C_{j,k}$ the hydrostatic restoring coefficient

F_j the complex amplitudes of the exciting force and moment. F_1, F_2 and F_3 are the amplitudes of the surge, sway and heave exciting forces, while F_4, F_5 and F_6 are the amplitudes of the roll, pitch and yaw exciting moments.

Since the ship has lateral symmetry (symmetric about the x, z plane), the generalized mass matrix, added-mass coefficients, damping coefficients and hydrostatic restoring coefficients are given by

$$M_{j,k} = \begin{bmatrix} M_{1,1} & 0 & 0 & 0 & 0 & 0 \\ 0 & M_{2,2} & 0 & 0 & 0 & 0 \\ 0 & 0 & M_{3,3} & 0 & 0 & 0 \\ 0 & 0 & 0 & M_{4,4} & 0 & 0 \\ 0 & 0 & 0 & 0 & M_{5,5} & 0 \\ 0 & 0 & 0 & 0 & 0 & M_{6,6} \end{bmatrix} \tag{2.2}$$

$$M_{1,1} = M = \rho \cdot \nabla \tag{2.3}$$

$$M_{2,2} = M = \rho \cdot \nabla \tag{2.4}$$

$$M_{3,3} = M = \rho \cdot \nabla \tag{2.5}$$

$$M_{4,4} = I_{xx} = k_{xx}^2 \cdot \rho \cdot \nabla \tag{2.6}$$

$$M_{5,5} = I_{yy} = k_{yy}^2 \cdot \rho \cdot \nabla \tag{2.7}$$

$$M_{6,6} = I_{zz} = k_{zz}^2 \cdot \rho \cdot \nabla \tag{2.8}$$

where

∇	volume of displacement
ρ	density of water
k_{xx}	radius of gyration in air for roll
k_{yy}	radius of gyration in air for pitch
k_{zz}	radius of gyration in air for yaw

$$A_{j,k}(or\ B_{j,k}) = \begin{bmatrix} A_{1,1} & 0 & 0 & 0 & A_{1,5} & 0 \\ 0 & A_{2,2} & 0 & A_{2,4} & 0 & A_{2,6} \\ 0 & 0 & A_{3,3} & 0 & A_{3,5} & 0 \\ 0 & A_{4,2} & 0 & A_{4,4} & 0 & A_{4,6} \\ A_{5,1} & 0 & A_{5,3} & 0 & A_{5,5} & 0 \\ 0 & A_{6,2} & 0 & A_{6,4} & 0 & A_{6,6} \end{bmatrix} \tag{2.9}$$

$$C_{j,k} = \begin{bmatrix} 0 & 0 & 0 & 0 & 0 & 0 \\ 0 & 0 & 0 & 0 & 0 & 0 \\ 0 & 0 & C_{3,3} & 0 & C_{3,5} & 0 \\ 0 & 0 & 0 & C_{4,4} & 0 & 0 \\ 0 & 0 & C_{5,3} & 0 & C_{5,5} & 0 \\ 0 & 0 & 0 & 0 & 0 & 0 \end{bmatrix} \tag{2.10}$$

The six coupled equations of motions reduce to two sets of equations: One set of three coupled equations for surge, heave and pitch, and another set of three coupled equations for sway, roll and yaw.

The coupled equations of motion for surge, heave and pitch can be written in the form

Surge motion equation

$$\left(M + A_{1,1}\right)\cdot \ddot{x}_1 + A_{1,5}\cdot \ddot{x}_5 + B_{1,1}\cdot \dot{x}_1 + B_{1,5}\cdot \dot{x}_5 = F_1 \tag{2.11}$$

Heave motion equation

$$\left(M + A_{3,3}\right)\cdot \ddot{x}_3 + A_{3,5}\cdot \ddot{x}_5 + B_{3,3}\cdot \dot{x}_3 + C_{3,3}\cdot x_3 + B_{3,5}\cdot \dot{x}_5 + C_{3,5}\cdot x_5 = F_3 \tag{2.12}$$

Pitch motion equation

$$\left(I_{yy} + A_{5,5}\right)\cdot \ddot{x}_5 + A_{5,1}\cdot \ddot{x}_1 + A_{5,3}\cdot \ddot{x}_3 + B_{5,1}\cdot \dot{x}_1 + B_{5,3}\cdot \dot{x}_3 + B_{5,5}\cdot \dot{x}_5 + C_{5,3}\cdot x_3 + C_{5,5}\cdot x_5 = F_5 \tag{2.13}$$

Another set of coupled equations of motion for sway, roll and yaw can be written in the form

Sway motion equation

$$\left(M + A_{2,2}\right)\cdot \ddot{x}_2 + A_{2,4}\cdot \ddot{x}_4 + A_{2,6}\cdot \ddot{x}_6 + B_{2,2}\cdot \dot{x}_2 + B_{2,4}\cdot \dot{x}_4 + B_{2,6}\cdot \dot{x}_6 = F_2 \tag{2.14}$$

Roll motion equation

$$\left(I_{xx} + A_{4,4}\right)\cdot \ddot{x}_4 + A_{4,2}\cdot \ddot{x}_2 + A_{4,6}\cdot \ddot{x}_6 + B_{4,2}\cdot \dot{x}_2 + B_{4,4}\cdot \dot{x}_4 + B_{4,6}\cdot \dot{x}_6 + C_{4,4}\cdot x_4 = F_4 \tag{2.15}$$

Yaw motion equation

$$\left(I_{zz} + A_{6,6}\right)\cdot \ddot{x}_6 + A_{6,2}\cdot \ddot{x}_2 + A_{6,4}\cdot \ddot{x}_4 + B_{6,2}\cdot \dot{x}_2 + B_{6,4}\cdot \dot{x}_4 + B_{6,6}\cdot \dot{x}_6 = F_6 \tag{2.16}$$

Since the ship has a long slender hull form, the hydrodynamic force associated with the surge motion is much smaller than the forces associated with the five other modes of motion. Hence, the three coupled equations of motion for surge, heave and pitch reduce to two coupled equations for pitch and heave.

2.2.2 Calculation of the Hydrodynamic Forces in Frequency Domain

Based on Newton's second law of dynamics, the equations of motion of a floating object in a seaway are rewritten:

$$\sum_{j=1}^{6} M_{i,j} \cdot \ddot{x}_j = F_i \qquad i = 1,2,\ldots 6 \tag{2.17}$$

where

F_i the sum of forces or moments acting in direction i

Under the assumption that the oscillatory motions are linear and harmonic, the harmonic wave exciting forces and moments are defined by

$$F_{wi}(\omega,t) = F_{wai}(\omega) \cdot \cos(\omega t + \varepsilon_{wi}(\omega)) \tag{2.18}$$

The hydromechanical forces and moments acting on the free floating object in wave consist of:

A) linear hydrodynamic reaction forces and moments expressed in terms with the hydrodynamic mass and damping coefficients:

$$-a_{i,j}(\omega) \cdot \ddot{x}_j(\omega,t) - b_{i,j}(\omega) \cdot \dot{x}_j(\omega,t) \tag{2.19}$$

B) linear hydrostatic restoring forces and moments expressed in a term with a spring coefficient:

$$-c_{i,j} \cdot x_j(\omega,t) \tag{2.20}$$

So the linear equations of motion become

$$\sum_{j=1}^{6} \left\{ \left(M_{i,j} + a_{i,j}(\omega)\right) \cdot \ddot{x}_j + b_{i,j}(\omega) \cdot \dot{x}_j(\omega,t) + c_{i,j} \cdot x_j(\omega,t) \right\} = F_{wai}(\omega) \cdot \cos(\omega t + \varepsilon_{wi}(\omega)) \tag{2.21}$$

If viscous effects are disregarded, the fluid motion can be assumed to be irrotional, so that the problem can be formulated in terms of potential-flow theory. The hydromechanical coefficients $a_{i,j}(\omega)$, $b_{i,j}(\omega)$ and $c_{i,j}$ in frequency domain can be calculated as shown in the coming section.

- **The Hydrodynamic Mass Coefficients in Frequency Domain**

The hydrodynamic mass coefficients are given by

$$a_{1,1} = \int_L m'_{1,1} \cdot dx_b \tag{2.22}$$

$$a_{1,5} = -\overline{BG} \cdot a_{1,1} \tag{2.23}$$

$$a_{2,2} = \int_L m'_{2,2} \cdot dx_b \tag{2.24}$$

$$a_{2,4} = \int_L m'_{2,4} \cdot dx_b + \overline{OG} \cdot a_{2,2} \tag{2.25}$$

$$a_{2,6} = \int_L m'_{2,2} \cdot x_b \cdot dx_b \tag{2.26}$$

$$a_{3,3} = \int_L m'_{3,3} \cdot dx_b \tag{2.27}$$

$$a_{3,5} = -\int_L m'_{3,3} \cdot x_b \cdot dx_b \tag{2.28}$$

$$a_{4,4} = \int_L m'_{4,4} \cdot dx_b + \overline{OG} \cdot \int_L m'_{4,2} \cdot dx_b + \overline{OG} \cdot a_{2,4} \tag{2.29}$$

$$a_{4,6} = \int_L m'_{4,2} \cdot x_b \cdot dx_b + \overline{OG} \cdot a_{2,6} \tag{2.30}$$

$$a_{5,5} = \int_L m'_{3,3} \cdot x_b^2 \cdot dx_b - \overline{BG} \cdot a_{1,5} \tag{2.31}$$

$$a_{6,6} = \int_L m'_{2,2} \cdot x_b^2 \cdot dx_b \tag{2.32}$$

$$a_{i,j} = a_{j,i} \tag{2.33}$$

where

$m'_{i,j}(\omega)$ the sectional hydrodynamic mass coefficient

x_b the longitudinal distance between cross-sections to centre of gravity, positive forwards;

$\overline{OG}$ the vertical distance of waterline to centre of gravity

$\overline{BG}$ the vertical distance of center of buoyancy to centre of gravity.

The remaining hydrodynamic mass coefficients are zero

- **The Damping Coefficients in Frequency Domain**

The damping coefficients are given by

$$b_{1,1} = \int_L n'_{1,1} \cdot dx_b \tag{2.34}$$

$$b_{1,5} = -\overline{BG} \cdot b_{1,1} \tag{2.35}$$

$$b_{2,2} = \int_L n'_{2,2} \cdot dx_b \tag{2.36}$$

$$b_{2,4} = \int_L n'_{2,4} \cdot dx_b + \overline{OG} \cdot b_{2,2} \tag{2.37}$$

$$b_{2,6} = \int_L n'_{2,2} \cdot x_b \cdot dx_b \tag{2.38}$$

$$b_{3,3} = \int_L n'_{3,3} \cdot dx_b \tag{2.39}$$

$$b_{3,5} = -\int_L n'_{3,3} \cdot x_b \cdot dx_b \tag{2.40}$$

$$b_{4,4} = \int_L n'_{4,4} \cdot dx_b + \overline{OG} \cdot \int_L n'_{4,2} \cdot dx_b + \overline{OG} \cdot b_{2,4} \tag{2.41}$$

$$b_{4,6} = \int_L n'_{4,2} \cdot x_b \cdot dx_b + \overline{OG} \cdot b_{2,6} \tag{2.42}$$

$$b_{5,5} = \int_L n'_{3,3} \cdot x_b^{\,2} \cdot dx_b - \overline{BG} \cdot b_{1,5} \tag{2.43}$$

$$b_{6,6} = \int_L n'_{2,2} \cdot x_b^{\,2} \cdot dx_b \tag{2.44}$$

$$b_{i,j} = b_{j,i} \tag{2.45}$$

where

$n'_{i,j}(\omega)$ the sectional hydrodynamic mass coefficient

The remaining hydrodynamic damping coefficients are zero.

- **The Spring Coefficients in Frequency Domain**

The spring coefficients are given by

$$c_{3,3} = 2 \cdot \rho \cdot g \cdot \int_L y'_w \cdot dx_b \tag{2.46}$$

$$c_{3,5} = -2 \cdot \rho \cdot g \cdot \int_L y'_w \cdot x_b \cdot dx_b \tag{2.47}$$

$$c_{4,4} = \rho \cdot g \cdot \nabla \cdot \overline{GM} \tag{2.48}$$

$$c_{5,5} = \rho \cdot g \cdot \nabla \cdot \overline{GM_L} \tag{2.49}$$

$$c_{i,j} = c_{j,i} \tag{2.50}$$

where

y'_w the sectional half breadth of waterline

$\overline{GM}$ the transverse metacentric height

$\overline{GM_L}$ the longitudinal metacentric height

2.2.3 Calculation of the Hydrodynamic Forces in Time Domain

As a result of the formulation in the frequency domain, any system influencing the behavior of the floating body should have a linear relation with the displacement, the velocity and the acceleration of the body. However, in many cases there are several complications which perish this linear assumption. To include these nonlinear effects in the vessel behavior, it is necessary to formulate the equations of motion in the time domain, which relates instantaneous values of forces, moments and motions.

Together with the hydrodynamic forces and moments, the linear restoring spring terms and the linear external loads, Newton's second law of dynamics provides the linear equations of motion in the time domain:

$$\sum_{j=1}^{6} \left\{ \left(M_{i,j} + A_{i,j} \right) \cdot \ddot{x}_j(t) + \int_0^{\infty} B_{i,j}(\tau) \cdot \dot{x}_j(t-\tau) + C_{i,j} \cdot x_j(t) \right\} = F_i(t) \tag{2.51}$$

where

$x_j(t)$ the translational or rotational displacement in direction at time t

$M_{i,j}$ the solid mass or inertia coefficient

$A_{i,j}$ the hydrodynamic mass coefficient in time domain

$B_{i,j}$ the retardation function in time domain

$C_{i,j}$ the spring coefficient in time domain

$X_i(t)$ the external load in direction i at time t

An easy method to determine $A_{i,j}$ and $B_{i,j}$, can be obtained by making use of the hydrodynamic mass and damping in the frequency domain. Ogilvie gave the relative simple relations, which can be found between $A_{i,j}$, $B_{i,j}$ and the calculated data of the hydrodynamic mass $a_{i,j}$ and damping $b_{i,j}$ in the frequency domain.

The retardation function $B_{i,j}$ is given

$$B_{i,j}(\tau) = \frac{2}{\pi} \cdot \int_0^\infty b_{i,j}(\omega) \cdot \cos(\omega\tau) \cdot d\omega \tag{2.52}$$

Hydrodynamic mass coefficient

$$A_{i,j} = a_{i,j}(\omega) + \frac{1}{\omega} \cdot \int_0^\infty B_{i,j}(\tau) \cdot \sin(\omega\tau) \cdot d\tau \tag{2.53}$$

This formula is valid for any value of ω, for $\omega = \infty$

$$A_{i,j} = a_{i,j} \tag{2.54}$$

2.3 Internal Mechanics

The analysis methods of internal mechanics can be categorized into four groups (ISSC 2003):

1) Empirical formulae
2) Simplified analytical approach
3) Simplified FEM
4) Nonlinear FEM

2.3.1 Empirical Formulae

Empirical formulae are useful for easy and quick estimation of the energy absorption of a ship in a collision or grounding accident. The first attempt to predict collision response was done by Minorsky (1959). He derived an empirical formula based on the volume of steel damaged. He followed a semi-analytical approach based on the past damage statistics (Speed, angle of encounter, displacements, drafts and location of damage). He derived the energy absorbed in collision as follows:

$$E = 414.5R_T + 121{,}900\left(Tons - knot^2\right) \tag{2.55}$$

R_T is defined as 'resistance factor':

$$R_T = \sum P_N L_N t_N + \sum P_n L_n t_n \tag{2.56}$$

where

P_N the depth of damage in N^{th} member of striking ship, ft

L_N the length of damage in N^{th} member of striking ship, ft

t_N the thickness of N^{th} member of striking ship, inches

P_n the depth of damage in N^{th} member of struck ship, ft

L_n the length of damage in N^{th} member of struck ship, ft

t_n the thickness of Nth member of struck ship, inch

From an engineering point of view, Minorsky's formula established a fairly consistent correlation between resistance factor and lost kinetic energy for high-energy collision.

Woisin(1979), Mcdermott et al. (1974) and Akita et al. (1972) modified the Minorsky's formula and gave the different empirical formulas. It is noted that empirical formulae are applicable only when the considered ship is similar to the ships used in the derivation of these formulae. The recent extensive studies on the structural crashworthiness have also produced many new simplified formulae that are believed to be more rationally and applicable to a wider range of problems such as grounding, ship-bridge collision and bottom raking of high speed crafts (Li 1999, Pedersen et al. 1998, Pedersen and Zhang 2000, Simonsen et al. 2004, Simonsen and Tornqvist2004, Wang and Yi 1997,Zhang 1999, Zhang et al. 2004)

2.3.2 Simplified Analytical Approach

This method is developed by analytical approach resulting in closed-form analytical formulations which can capture the basic features of structural crashworthiness. The idea is that the work rate (power) of an external force must equal the rate of internal energy dissipation in the structure. The procedure is to find the kinematically admissible deformation of the structure that yields the lowest force - "least upper bound".

The basic assumptions of the method are:

- Collision is assumed to be a quasi-static process.

- Material dynamic effects (strain rate sensitivity) are taken into account by assuming a yield flow stress σ_o, defined as:

$$\sigma_o = \frac{\sigma_y + \sigma_u}{2} \tag{2.57}$$

- The material is assumed to be rigid-perfectly plastic.

The simplified analytical approach consists of four major steps as follows.

1) Identify primary damage patterns of structural components according to observation of actual damage
2) Develop idealized theoretical models and derive theoretical formulations to capture the main features of the damage patterns
3) Establish global models for the entire damage process of the ship hull
4) Combine the global damage models with formulations for individual structural components

Wang (1995) identified six different structural failure modes involved in ship collision and grounding.

2.3.2.1 Tearing of Plate

When a wedge with an angle 2θ advances into a metal sheet, the plate separates ahead of the wedge tip and curves into two surfaces of variable curvature (Fig. 2.2).

The cutting force F has the following expression:

$$F = 1.51\sigma_0 t^{1.5} l^{0.5} (\sin\theta)^{0.5} \left(1 + \frac{\mu}{\tan\theta}\right) \tag{2.58}$$

where

σ_0 the material flow stress

l the tearing length

t the plate thickness

θ the semi-angle of the wedge

μ the friction coefficient

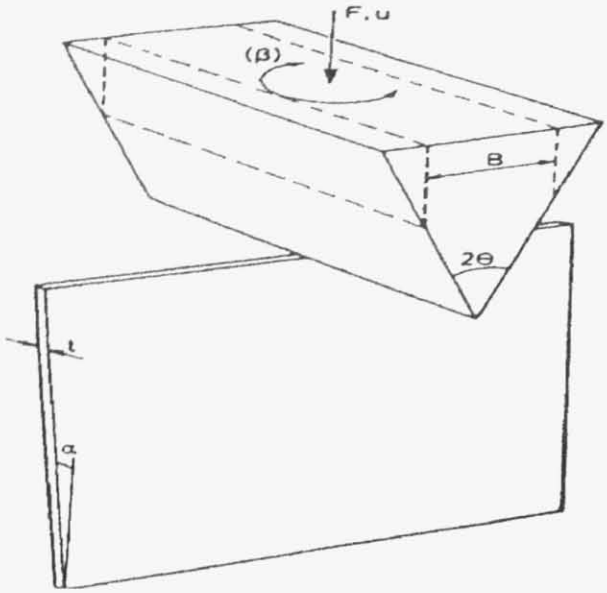

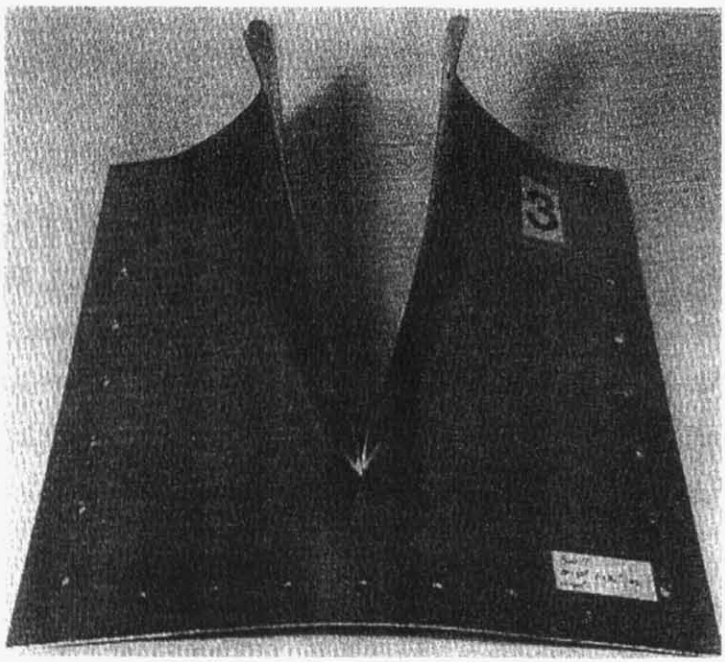

Fig. 2.2 Schematic and picture of plate cutting experiment(Thomas, 1992)

2.3.2.2 Concertina Tearing of Plate

When loaded by edge load, a plate may pile up in front of the wedge and be tore at some remote location (Fig. 2.3)

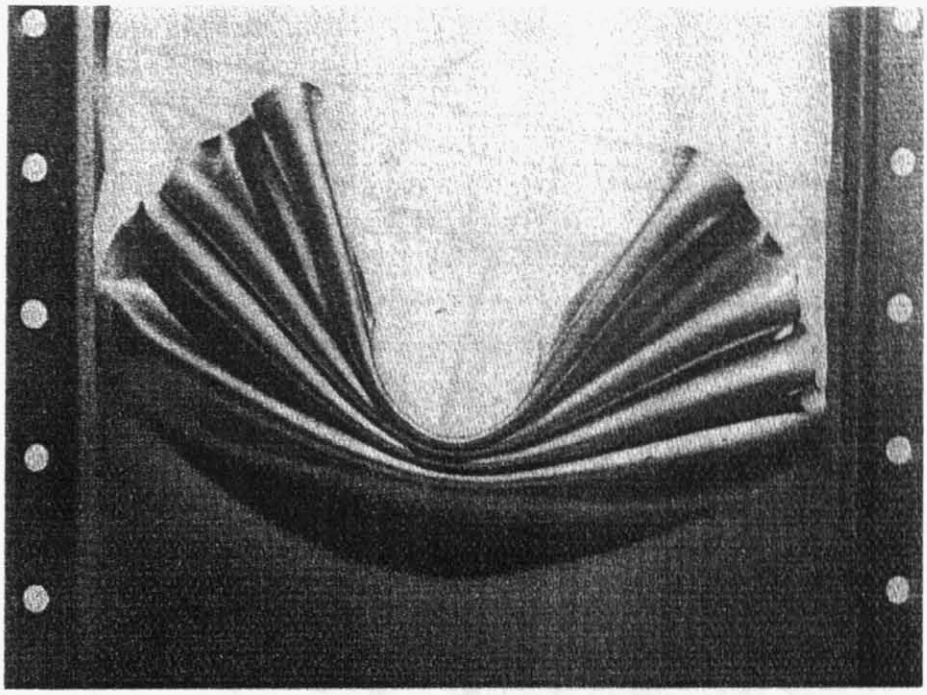

Fig. 2.3 A typical picture of concertina tearing of plate

The mean indention force F_m has the following expression:

$$F_m = 4.5\sigma_0 t^{1.67}(2b)^{0.33} \tag{2.59}$$

where

σ_0 the material flow stress

t the plate thickness

$2b$ the width of the plate

2.3.2.3 Denting of Plate

The existence of transverse structure (such as floor in ship bottom) makes the plate behave in quite a different way from the tearing of plate. The failure of the plate is due to local denting (Fig. 2.4)

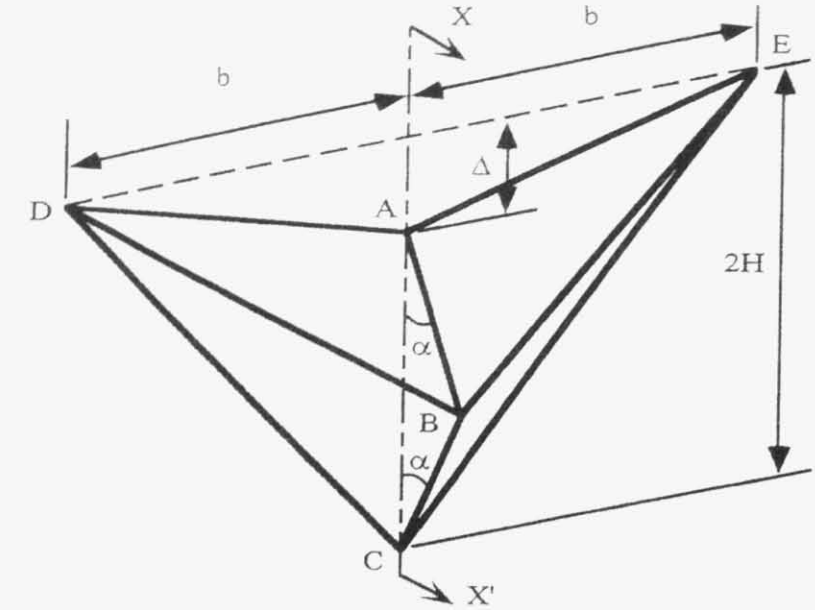

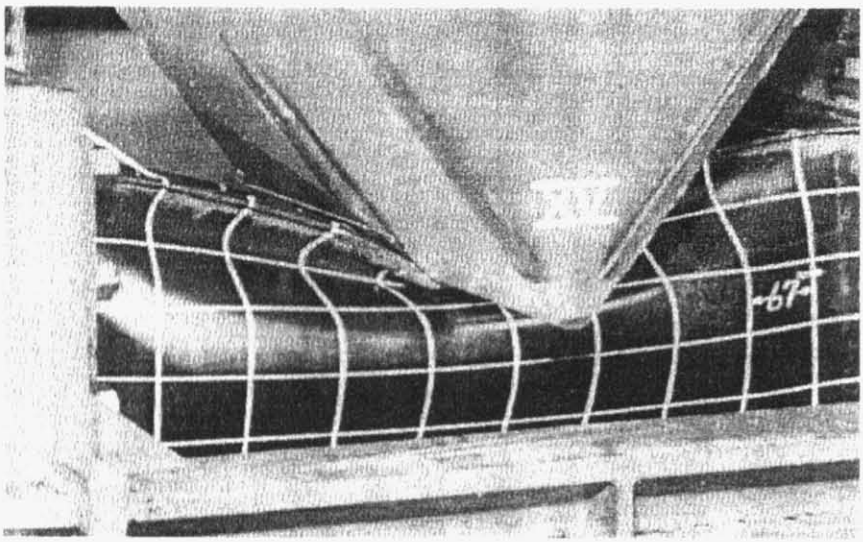

Fig. 2.4 Kinematic model and picture for denting of plate

The mean resistance force F_m has the following expression:

$$F_m = 2.32\sigma_0 t^{1.67}(2b)^{0.33} \tag{2.60}$$

where

σ_0 the material flow stress

t the plate thickness

$2b$ the width of the plate

2.3.2.4 Penetration of Plate

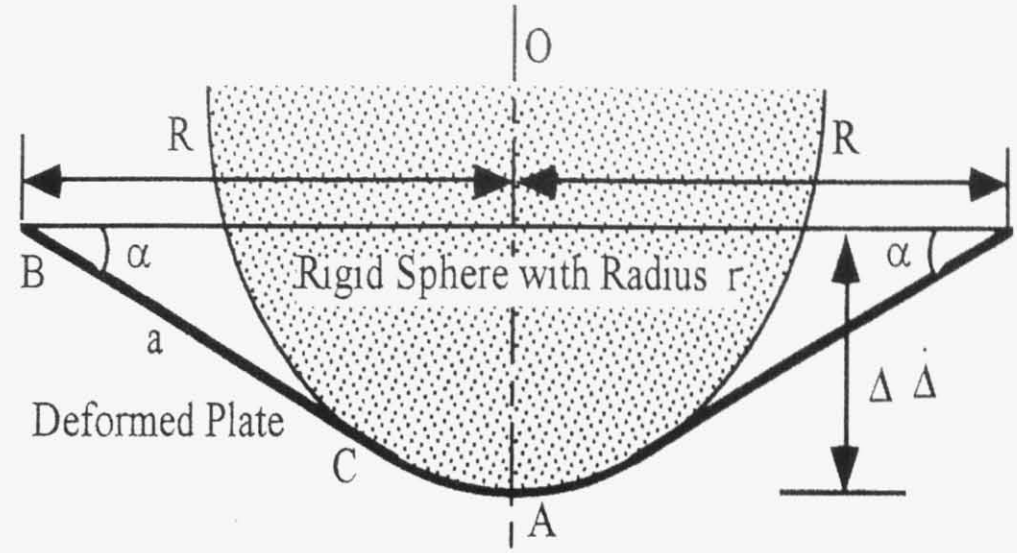

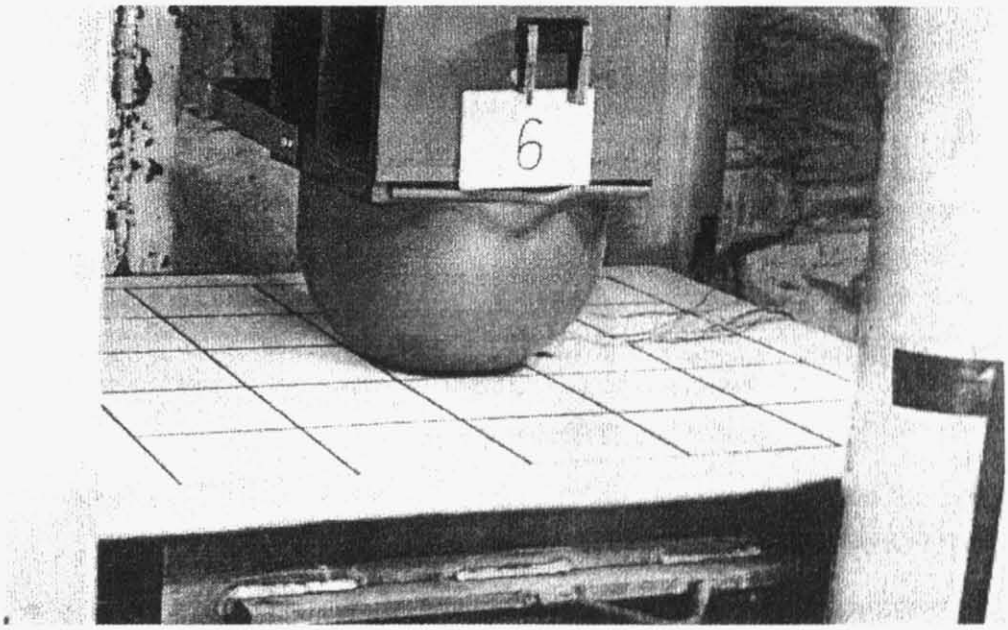

Fig. 2.5 Kinematic model and picture for penetration of plate

When the metal plate subjected to the indentation of a rigid ball (Fig. 2.5), the indentation load F has the following expression:

$$F = \pi\sigma_0 tR\sin\alpha\cdot\left(1+\frac{r}{R}\sin\alpha\right) \tag{2.61}$$

where

σ_0 the material flow stress

t the plate thickness

R the radius of the plate

r the radius of the rigid sphere

2.3.2.5 Stretching of Plate

If a plate is subjected to lateral load which is mainly along a line, it stretches to resist the indentation. This behavior is similar to that of a beam (Fig 2.6)

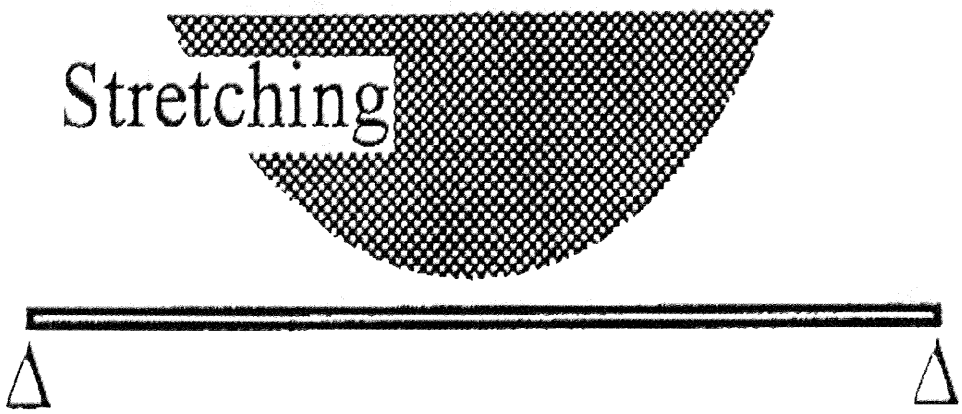

Fig. 2.6 Stretching of plate

For a plate which has a span of $2L$, width of B, thickness t, and deformed to Δ at its mid-span, its resistance has the following expression:

$$F = 2\sigma_0 Bt \sin\alpha \approx 2\sigma_0 Bt \frac{\Delta}{L} \tag{2.62}$$

2.3.2.6 Axial Crushing of Thin-Walled Structure

During the ship collision and grounding, the crushing collapse of thin-walled structure subjected to compressive load is one of the important failure modes. When thin-walled structure subjected to axial load, it will collapse either in symmetrical pattern or in non-symmetrical pattern. Fig. 2.7 shows the formation of such folds in a crushed square tube.

Jones and Birch(1990) derived the mean crushing force as the following expression:

$$F_m = \frac{2.3910}{\eta}\left(\frac{t}{b}\right)^{2/3}\sigma_0 A \tag{2.63}$$

where

η ratio of effective crushing length

b the breadth of tube

t the thickness of plate

A the cross-sectional area of tube

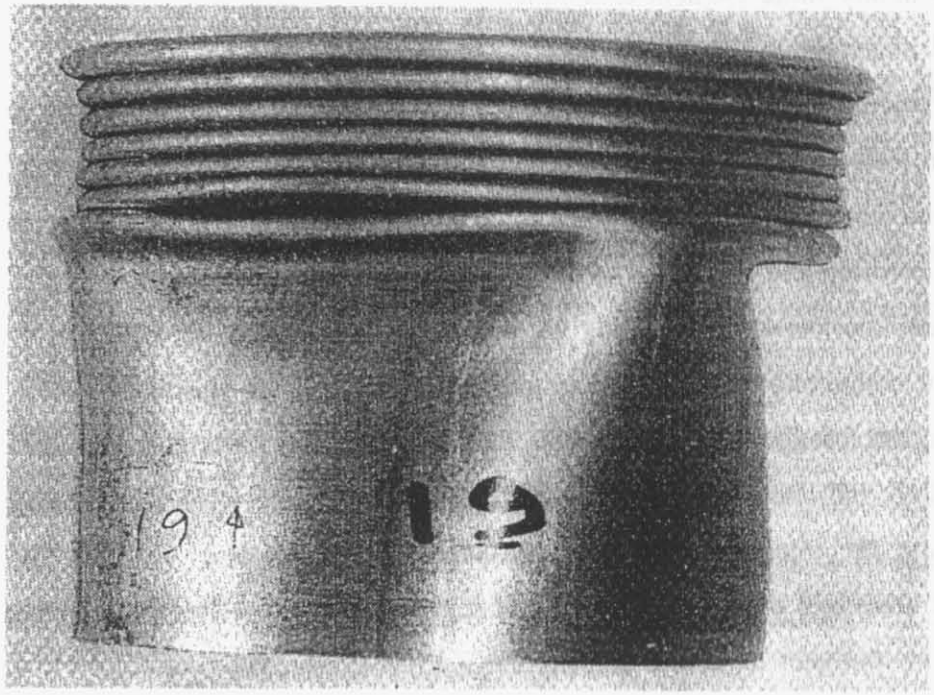

Fig. 2.7 A typical picture of axial crushing of tube

Applications of this advanced methodology to various collision and grounding situations were summarized extensively by the ISSC 2003 Committee V.3 This approach has the advantage of capturing the basic characteristics of structural crashworthiness with minimized structural modeling efforts. A series of methods have been developed using this advanced technology. (Brown 2002, Han et al. 2005, Kitamura 1999, Liang et al. 2000, McDermott et al 1974, Paik et al 1994, 1995,1997, Pedersen et al 1993, 2000, Ohtsubo et al 1995, Simonsen et al. 1997, 2000, 2004, Suzuki et al. 1995, 2000, 2001, Tikka 2001, Urban 2003, Wang et al 1997, 1998, 1999, 2000, 2002a, 2002b, Wierzbicki et al 1983, 1993, 1995,Woisin 1998, 1999, Xiao et al. 2001, Yang et al 1988, Yu 1996, Zhang 1999, 2002, Zhang and Wu 1990, Zhu et al. 1996, 1998).

2.3.3 Simplified FEM

Paik and Pederson (1994) used the Idealized Structural Unit Method (ISUM) as a nonlinear analysis tool for collision and grounding problems. This approach often combines the analytical models for crushing, tearing and yielding behavior of structural components, and the ordinary finite element technique. To determine these forces, the outer and inner side shell plates around the colliding zone of the struck ship are modeled by membrane tension triangular/rectangular plate units with a stiffness matrix formulated by considering the rupture behavior. Transverse webs and side stringers that connect the outer and inner hulls are modeled by rectangular plate units, which are formulated by taking into account yielding, crushing and rupture. The striking ship was modeled as a rigid body. Dynamic effects were considered by including the influence of strain-rate sensitivity in the material model. The computing cost and modeling efforts of analysis are reasonably small, while the accuracy is not lost (Ito et al. 1984, 1986, Paik and Pedersen 1996, Paik et al. 1999, Paik et al. 2002, Paik and Thayamaballi 2002). This group of techniques has the advantage of FEM in modeling the interactions between structures involved, and also has the merit of simplified analytical methods in dealing with complex damage behavior. Since the rapid advances in computer hardware and nonlinear FEM codes, the simplified FEM has been very few activities nowadays.

2.3.4 Nonlinear FEM

Recent advances in computers and calculation algorithms have made nonlinear finite element analysis become an available tool for assessing the internal mechanics of ship collisions and groundings. Two types of FE methodologies, implicit and explicit techniques, are relevant. Implicit methodologies solve systems of equations, and the calculation cost depends largely on the equation solver and the computer capacity, especially memory resources. Implicit methodologies based codes include ABAQUS/Standard, ANSYS, MARC and NASTRAN. However, explicit systems do not require equation solving. Equilibrium is solved in the element level, which requires very small time steps to comply with stability requirement for equation solving. Explicit methodologies based computer codes include ABAQUS/Explicit, DYTRAN, LS-DYNA, PAMCRASH and RADIOSS. One of the pioneering studies involving finite-element simulations has been performed by

Vredeveledt et al (1993). Those numerical simulations have considered the collision adequacy of inland vessels using MSC/Dytran. Application of nonlinear FEM simulation has been the main theme of recent studies (Wu et al. 2004, Zhang L. et al. 2004, Endo et al. 2001,2004, Yamada et al 2004, 2005, Jiang et al 2004, Tornqvist et al. 2004, Wang et al. 2003, 2002b, Le Sourne et al. 2003, Kajaste-Rudnitski 2004a, 2004b and 2005, Nolau Neto et al. 2004, Jastrzebski et al. 2004, Lehmann et al. 2004, Konter et al. 2004, Oh et al. 2005, Liu et al. 2003, Klanac et al. 2005, Ozguc at al. 2005, Hu et al. 2005, Alsos et al. 2005).

The reliability of the numerical simulation results largely depends on the proper definition of problem and careful control of some critical parameters in FEM code. In chapter 3 and 4, the experiments of Axial Crushing of Thin-Walled Structure and single bottom grounding are used to validate the accuracy and stability of the nonlinear FEM.

2.4 Remarks

Although the technologies have advanced remarkably, many areas related to the mechanics of collision and grounding still need to be improved or explored further. Nevertheless, the question of how to calculate oil tanker's response in an accident continues to be central to today's research and development.

Some important R & D topics are proposed as below:

1) Guidelines for non-linear FEM analyses, which include critical element size, dynamic material models and fracture criteria.
2) Benchmark studies on simplified analytical models, numerical methods and experimental results for collisions and grounding.
3) Studies on the influence of fluid in tanks.
4) Studies on coupled external and internal mechanics.
5) Fracture criteria to be used in crushing and tearing analyses by either full non-linear FEM or simplified analytical methods.

Chapter 3 Numerical Analysis of Simple Component Failure Mode Axial Crushing of Thin-Walled Structure

3.1 Previous Researches

During the ship collision and grounding, the crushing collapse of thin-walled structure subjected to compressive load is one of the important failure modes. The relevant research work was begun since 1980s. Jones&Brich(1990) performed small-scale experiments and also gave the empirical formula of the mean crushing load. Wierzbicki et al(1983), Ohtsubo& Suzuki(1994), Paik& Pedersen(1995) gave the formulas for the mean crushing load by using the upper bound plasticity theorem. The classical theorem can be formulated as follow:

If the work rate of a system under the applied loads during any kinematically admissible collapse of the structure is equated to the corresponding internal energy dissipation rate, then this system under the applied loads will cause, or be at the point of collapse.

Paik et al (1996) performed a series of experiments on quasi-static crushing of stiffened square tubes and brought forward an empirical formula for the mean crushing load .The load speed was kept less than 0.05mm/sec to simulate the quasi-static load condition and neglect the dynamic effect. Table 3.1 shows tensile test results of different plate thickness and Table 3.2 shows dimensions and results of some test specimens. Fig. 3.1 shows four types of test specimens in the experiment: unstiffened square tube (US), longitudinally stiffened square tube (LS), transversely stiffened square tube (TS), orthogonally stiffened square tube (OS).

Table 3.1 Tensile test results of different plate thickness

Plate Thickness (mm)	Density (kg/m3)	Elastic Modulus (GPa)	Poisson Ratio	Yield Strength (MPa)	Ultimate Stress (MPa)	Fracture Strain
2.1	7860	200.1	0.3	328.5	399.4	0.374
2.2	7860	199.2	0.3	286.1	351.9	0.419
2.8	7860	205.8	0.3	310.8	363.3	0.354
3.0	7860	207.8	0.3	299.3	351.2	0.356
3.2	7860	209.7	0.3	427.6	477.2	0.249
4.2	7860	199.9	0.3	366.8	450.8	0.365

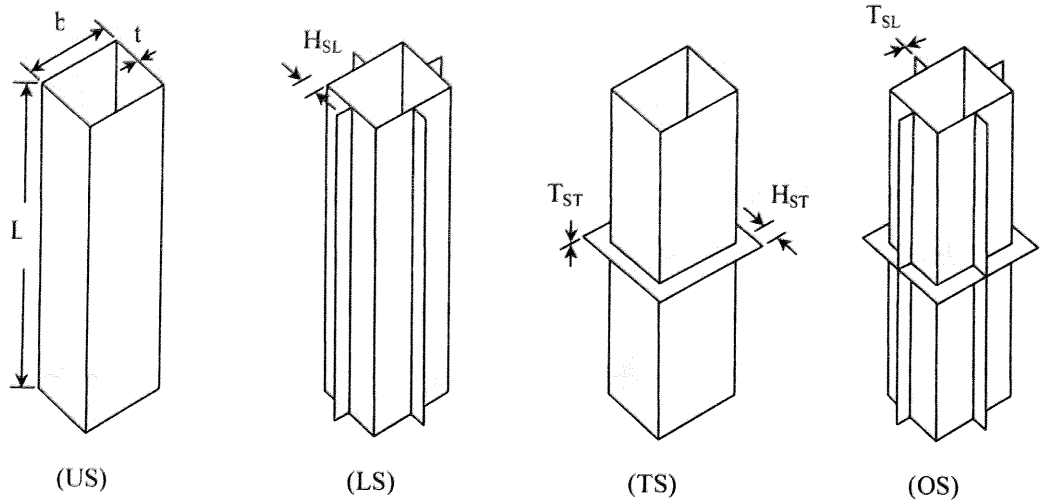

Fig. 3.1 Four types of stiffened square tube specimens

As previously noted, the stiffeners will affect the mean crushing strength of stiffened structure. If the unstiffened tube has the same energy absorption capability as the stiffened tube, we think that the thickness of unstiffened tube is the equivalent plate thickness of stiffened tub. Then the stiffened tube is replaced by an unstiffened tube with the equivalent plate thickness. The widely used equivalent plate thickness equation is as follows:

$$t_{eq} = t + \frac{A_l}{4b} \tag{3.1}$$

where

t the thickness of tube

$A_l = N_L \times T_{SL} \times T_{SL}$ the sectional area of longitudinal stiffeners

b the breadth of tube

Some formulas for the mean crushing load of square tube are as follows:

Jones & Birch(1990)

$$P_m = \frac{2.3910}{\eta}\left(\frac{t_{eq}}{b}\right)^{2/3}\sigma_0 A \tag{3.2}$$

where

η the ratio of effective crushing length

σ_0 the yield strength of material

A the cross-sectional area of tube

Table 3.2 Dimensions and results of some test specimens

Test No.	L (mm)	b (mm)	t (mm)	T_{SL} (mm)	H_{SL} (mm)	T_{ST} (mm)	H_{ST} (mm)	N_L	N_T	A_l [1] (mm^2)	A_t [2] (mm^2)	P_u (kN)	P_m (kN)	L' (mm)	η
US-2	450	100	2.8	-	-	-	-	-	-	-	-	337.12	100.98	108	0.76
LS-1	450	100	2.8	2.8	20.0	-	-	4	-	224	-	481.18	161.66	167	0.63
LS-2	450	100	2.8	2.8	30.0	-	-	4	-	336	-	522.34	201.08	140	0.69
LS-4	450	100	2.8	2.8	40.0	-	-	4	-	448	-	595.84	229.74	153	0.66
LS-7	450	100	2.8	2.8	15.0	-	-	4	-	168	-	447.86	133.87	153	0.66
LS-8	450	100	2.8	2.8	15.0	-	-	8	-	336	-	533.12	206.16	153	0.66
TS-1	450	100	2.8	-	-	2.8	20	-	4	-	224	337.12	105.56	113	0.75
TS-2	450	100	2.8	-	-	2.8	30	-	4	-	336	331.24	118.83	131	0.71
TS-3	450	100	2.8	-	-	2.8	40	-	4	-	448	346.92	110.39	117	0.74
TS-4	450	100	2.8	-	-	2.8	20	-	8	-	448	329.28	116.77	126	0.72
TS-5	450	100	2.8	-	-	2.8	30	-	8	-	672	338.59	132.50	135	0.70
TS-6	450	100	2.8	-	-	2.8	40	-	8	-	896	340.55	127.98	131	0.71
TS-7	450	100	4.2	-	-	4.2	20	-	4	-	224	661.50	268.42	135	0.70
TS-8	450	100	4.2	-	-	4.2	20	-	8	-	448	685.02	294.42	149	0.67
OS-1	450	100	2.8	2.8	20	2.8	20	4	4	224	224	476.77	185.73	153	0.66
OS-13	450	100	2.8	2.8	15	2.8	15	4	4	168	168	454.23	150.23	135	0.70
OS-14	450	100	2.8	2.8	15	2.8	15	4	8	168	336	454.72	195.32	135	0.70
OS-15	450	100	2.8	2.8	15	2.8	15	8	4	336	168	527.24	201.55	149	0.67
OS-16	450	100	2.8	2.8	15	2.8	15	8	8	336	336	535.57	220.62	149	0.67

1) $A_l = N_L \times T_{SL} \times T_{SL}$ 2) $A_t = N_T \times T_{ST} \times T_{ST}$

Paik(1996)

$$P_m = \frac{1}{\eta}\left\{1.4245\left(\frac{t_{eq}}{b}\right)^{0.5} + 0.2673\left(\frac{t_{eq}}{b}\right)\right\}\sigma_0 A \tag{3.3}$$

Lee & Choung(1996)

$$P_m = \frac{0.1250 C_L}{\eta}\left\{0.7622\left(\frac{t_{eq}}{b}\right)^{1/6} + 14.9110\left(\frac{t_{eq}}{b}\right)^{2/3}\right\}\sigma_0 A$$

$$C_L = 0.0375 N_L + 1.0 \tag{3.4}$$

where

C_L the influence coefficient of longitudinal stiffeners.

Paik et al (1996) gave the empirical equation for the ratio of effective crushing length η

For unstiffened tube and transversely stiffened tube

$$\eta = 0.728 \tag{3.5}$$

For longitudinally or orthogonally stiffened tube

$$\eta = 0.728 \qquad \text{if } 0 \le \frac{t_{eq}}{b} \le 0.0336 \tag{3.6}$$

$$\eta = 704.49\left(\frac{t_{eq}}{q}\right)^2 - 81.22\left(\frac{t_{eq}}{b}\right) + 2.66 \quad \text{if } 0.0336 \le \frac{t_{eq}}{b} \le 0.055 \tag{3.7}$$

In general, when the structures have the same equivalent plate thickness, the same mean crushing strengths are considered. However the experimental data show that the mean crushing strength of the different stiffened tubes are quite different, which even have the same equivalent plate thickness. Fig. 3.2 shows the comparison of formulas of the mean crushing load with experimental results, the present equivalent plate thickness formula does not take the effect of the stiffeners into account perfectly, especially the influence of transverse stiffeners.

Experimental data obtained by Paik et al (1996)showed that the mean crushing loads of orthogonally stiffened tubes, which have the same longitudinal stiffeners but different transverse stiffeners, are quite different. Obviously, the influence of the transversely stiffeners on the mean crushing load should be taken into account.

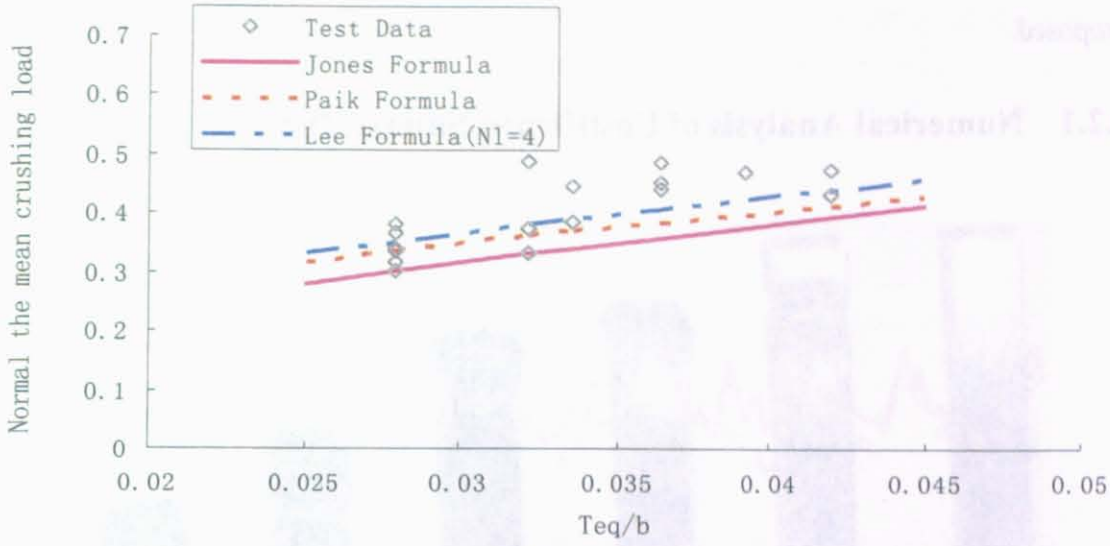

Fig. 3.2 Comparison of previous formulation with experimental results

3.2 Numerical Analysis of Stiffened Square Tube

In this section, a study on the mean crushing strength of square tube is performed using nonlinear FEM. The new formulas of the equivalent plate thickness and the mean crushing load are derived. The procedure is done in the following way:

First, one unstiffened tube specimen (for example US-2) is taken as model to set up FE model and calculate. Three main parameters, which are the energy curve, the mean crushing load and progressive damage, are considered to compare the numerical simulation with the test results. The aim of this step is to determine the parameters in the FE model.

Secondly, maintaining other parameters of FE model, a series of calculations are performed with different thicknesses of plate to get a series of the displacement-the crushing load curves. The plate thickness-the mean crushing load curve can also be drawn.

Thirdly, the experimental data of longitudinal stiffened tube is compared with numerical simulation results of unstiffened square tube. When the numerical simulation result is coincident with the test data of one longitudinally stiffened square tube, it is considered that the plate thickness of numerical simulation is the equivalent plate thickness of the longitudinal square tube. The same method is also applied in the transversely stiffened and orthogonally tubes. The new equivalent plate thickness formula is derived

Finally, using the new equivalent plate thickness formula and the test results of the mean crushing loads, new formula for the ultimate load and mean crushing load is

proposed.

3.2.1 Numerical Analysis of Unstiffened Square Tube

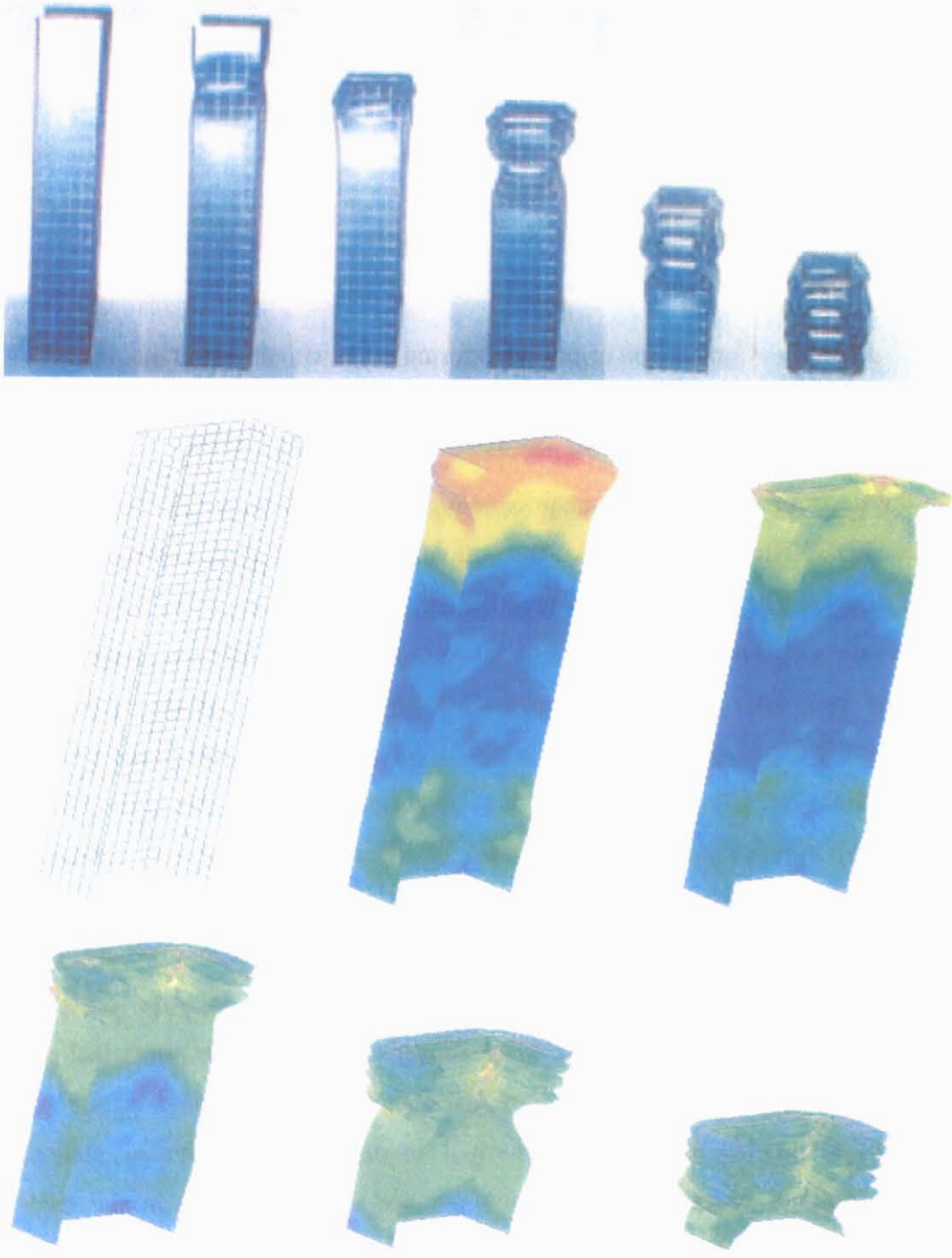

Fig. 3.3 Progressive collapse comparison for unstiffened square tube

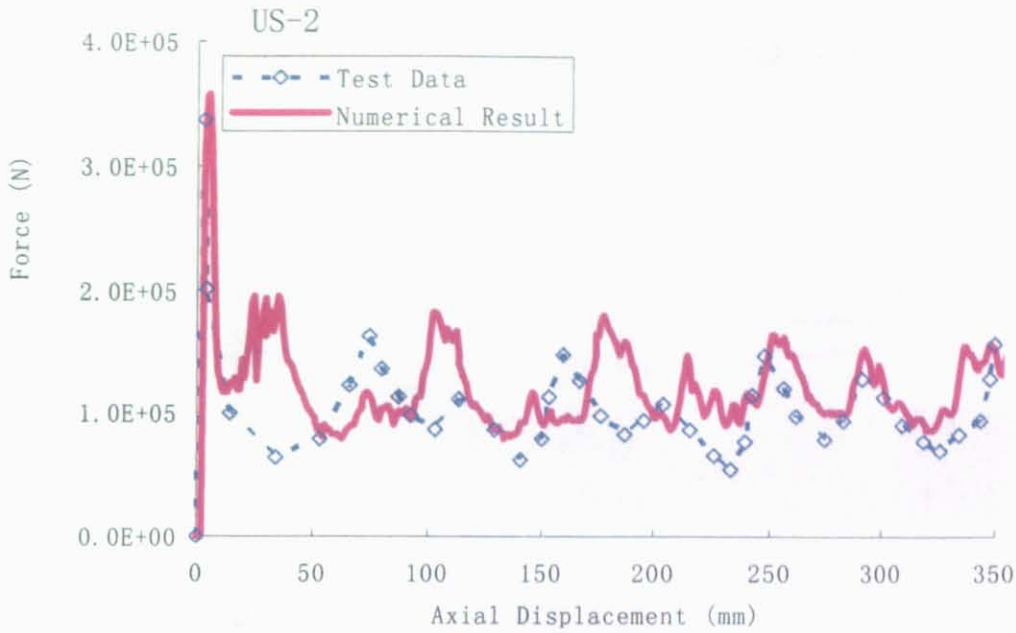

Fig. 3.4 Crushing force curve of unstiffened square tube

Table 3.3 Comparison of numerical results with experimental (US-2) results

	P_u (kN)	P_m (kN)
Experimental Results	337.12	100.98
Numerical Results	357.23	101.32

The test specimen US-2 is selected here for comparison. Fig. 3.3 and Fig. 3.4 show the progressive collapse and crushing force curve of unstiffened square tube. Table 3.3 shows the comparison of the numerical results and experimental results.

Maintaining other parameters of FE model, a series of calculations are performed with different thicknesses of plate and a series of the displacement-the crushing load curves are obtained. Fig. 3.5 shows the mean crushing load and ultimate load curve with different plate thicknesses, which are changed from 2.8mm to 4.3mm. It is very interesting that the distributions of numerical results of the mean crushing load and ultimate load are nearly linear. The empirical equation of the mean crushing load can be derived by normalizing the equivalent plate thickness when the ratio range of the equivalent plate thickness to the breadth is from 0.028 to 0.043. Similarly the empirical equation of the ultimate load is also derived from Fig. 3.5 as follows:

$$P_u = 1.547 \times 10^4 \cdot \frac{t_{eq}}{b} - 20.84 \qquad 0.028 \le \frac{t_{eq}}{b} \le 0.043 \qquad (3.8)$$

$$P_m = 1.041 \times 10^4 \cdot \frac{t_{eq}}{b} - 187.14 \qquad 0.028 \le \frac{t_{eq}}{b} \le 0.043 \qquad (3.9)$$

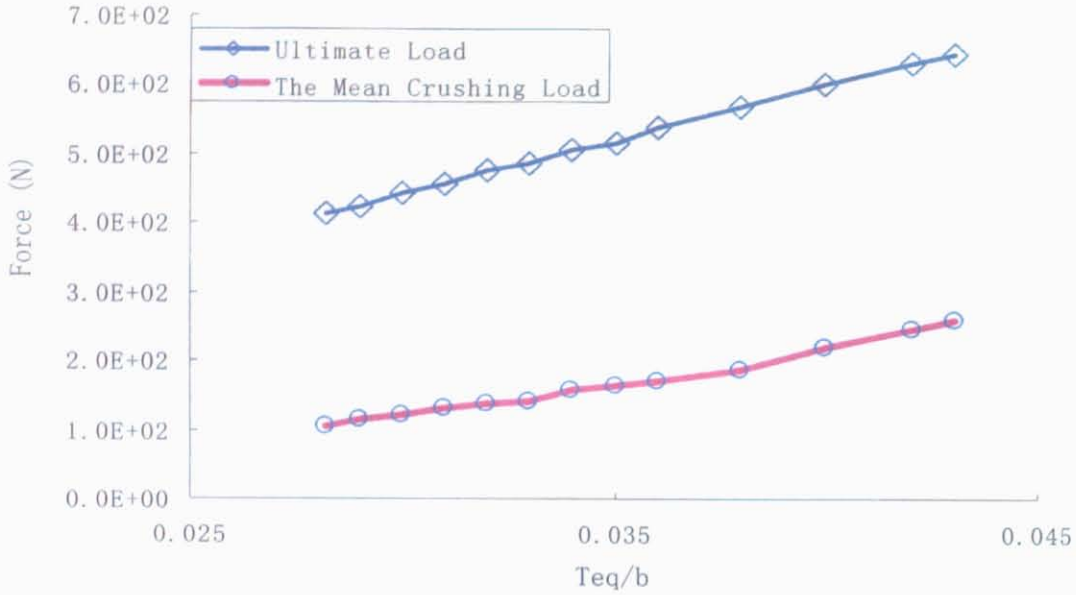

Fig. 3.5 Mean crushing load and ultimate load curve with different plate thickness

3.2.2 Numerical Analysis of Longitudinally Stiffened Square Tube

The specimen LS-7 is selected here for comparison. Table 3.4 shows the comparison of the experimental results, the numerical results with longitudinally stiffened tube model and equivalent unstiffened tube model. Fig. 3.6 and Fig. 3.7 show the progressive collapse and crushing force curve of longitudinally stiffened square tube.

Table 3.4 Numerical results for longitudinally stiffened square tube

	P_u (kN)	P_m (kN)
Experimental results	447.86	133.87
Numerical results (Longitudinally Stiffened Tube Model)	467.17	134.70
Numerical results (Equivalent US Model, 3.1mm)	458.73	131.30

There are five test specimens for the longitudinally stiffened square tube. Based on the experimental results and compared with Fig. 3.5, a series of the equivalent plate thicknesses

are determined respectively. Table 3.5 shows the equivalent plate thicknesses of longitudinally stiffened square tube.

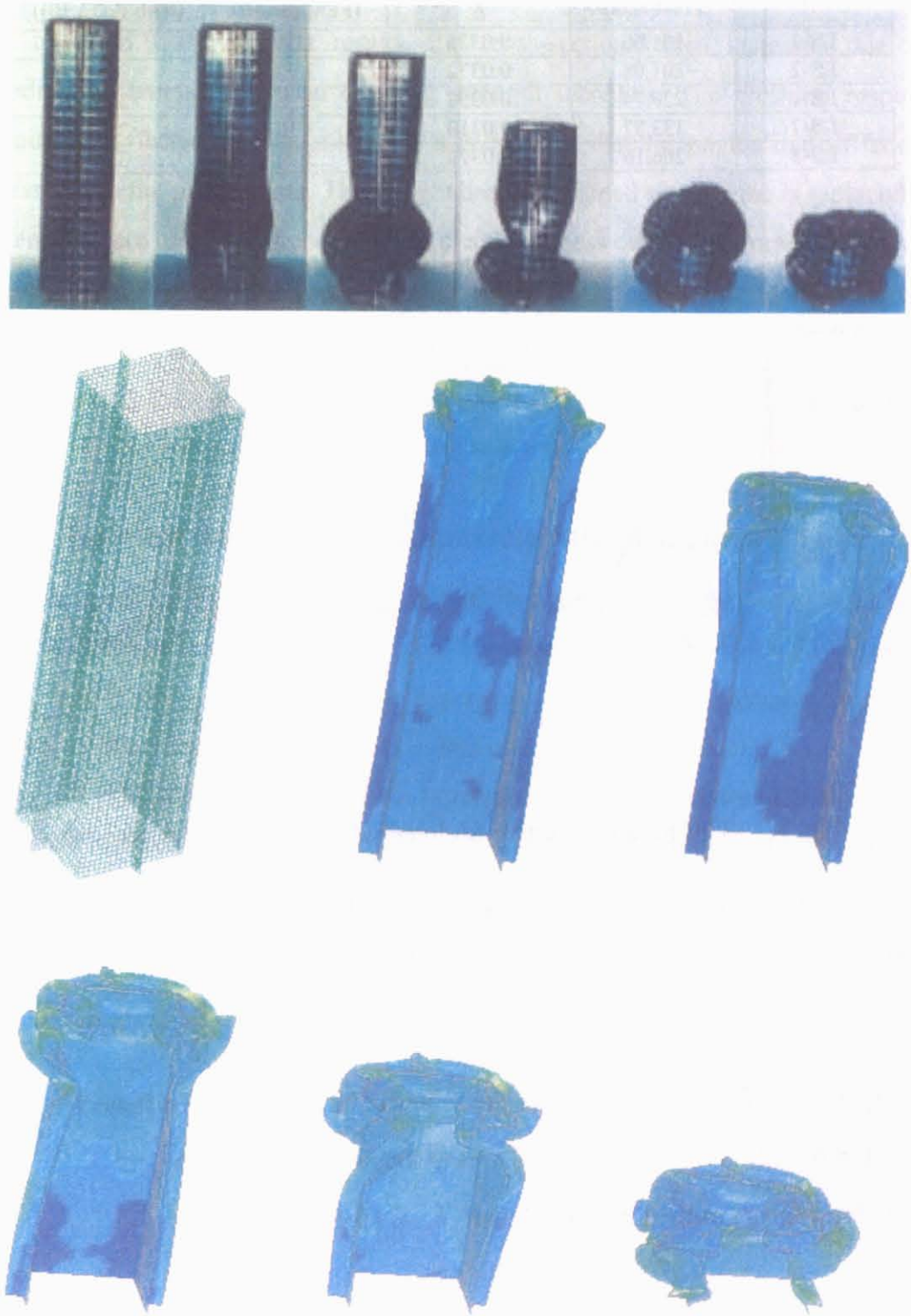

Fig. 3.6 Progressive collapse comparison for longitudinally stiffened square tube

Table 3.5 Equivalent plate thicknesses for longitudinally stiffened square tube

Specimen No.	P_m (kN) (Test data)	$\frac{t_{eq}^{fem}}{b}$	t_{eq}^{fem} (mm) (FEM results)	t_{eq} (mm) (with Eq.(3.10))
LS-1	161.66	0.0335	3.35	3.39
LS-2	201.08	0.0372	3.72	3.68
LS-4	229.74	0.0398	3.98	3.98
LS-7	133.87	0.0310	3.10	3.24
LS-8	206.16	0.0374	3.74	3.68

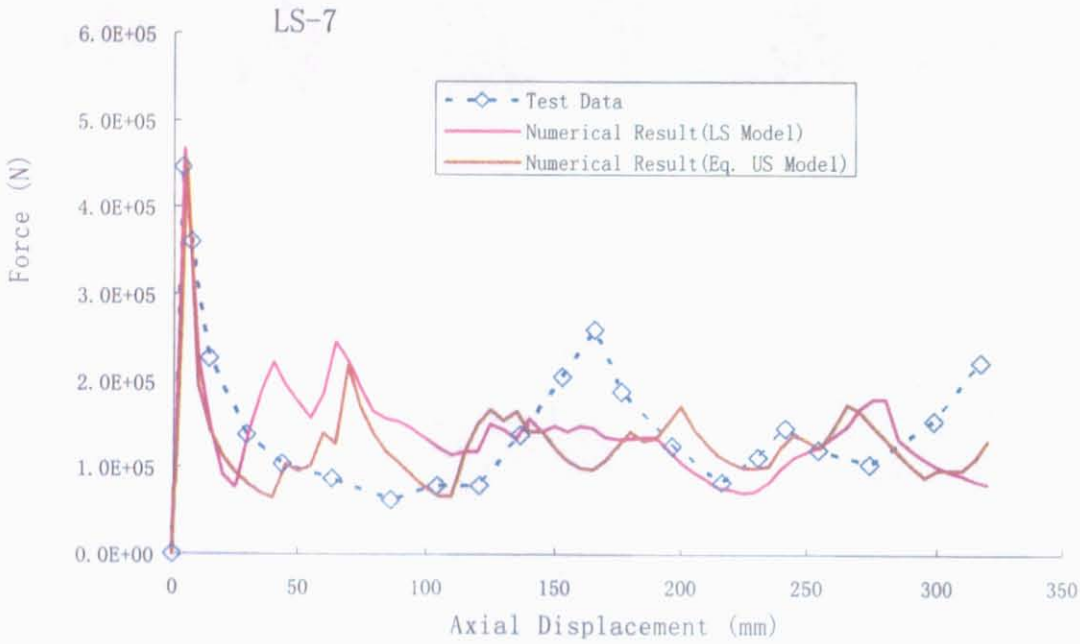

Fig. 3.7 Crushing force curve for longitudinally stiffened square tube

Referring to equation (3.1), the new equivalent plate thickness formula for longitudinally stiffened square tube is given as follows:

$$t_{eq} = t + k_l \frac{A_l}{4b} \qquad 0.028 \le \frac{t_{eq}}{b} \le 0.043 \qquad (3.10)$$

where: k_l : the coefficient accounting for the influence of longitudinal stiffeners

$A_l = N_L \times T_{SL} \times H_{SL}$: the sectional area of longitudinal stiffeners

Using least square method, the coefficient k_l is given as follows

$$k_l = \frac{\sum_{i=1}^{5}\left(t_{eq}^{fem}(i)A_l(i)\right) - \sum_{i=1}^{5}\left(tA_l(i)\right)}{\frac{1}{4b}\sum_{i=1}^{5}\left(A_l(i)\right)^2} \tag{3.11}$$

As observed from the test results, the cross-sectional area increases due to the longitudinal stiffeners, the mean crushing strength increases. The crushing response is predominantly affected by plate thickness. It is apparent that the longitudinal stiffeners can be smeared into the parent plate. The longitudinally stiffened square tube is replaced by an unstiffened square tube with the equivalent plate thickness calculated from equation (3.10). Where k_l is an empirical constant accounting for the influence due to the longitudinal stiffeners. In this study, based on the equivalent plate thickness data determined by FEM simulation result, the coefficient k_l is taken as 1.05, which is calculated from equation (3.11).

3.2.3 Numerical Analysis of Transversely Stiffened Square Tube

The test specimen TS-7 is selected here for comparison. Fig. 3.8 and Fig. 3.9 show the progressive collapse and the crushing force curve of transversely stiffened square tube. Table 3.5 shows the comparison of the experimental results, the numerical results with transversely stiffened tube model and equivalent unstiffened tube model.

There are eight test specimens for the transversely stiffened square tube. Based on the experimental results and compared with Fig. 3.5, a series of the equivalent plate thicknesses are determined respectively. Table 3.7 shows the equivalent plate thicknesses of transversely stiffened square tube.

Fig. 3.8 Progressive collapse comparison for transversely stiffened square tube

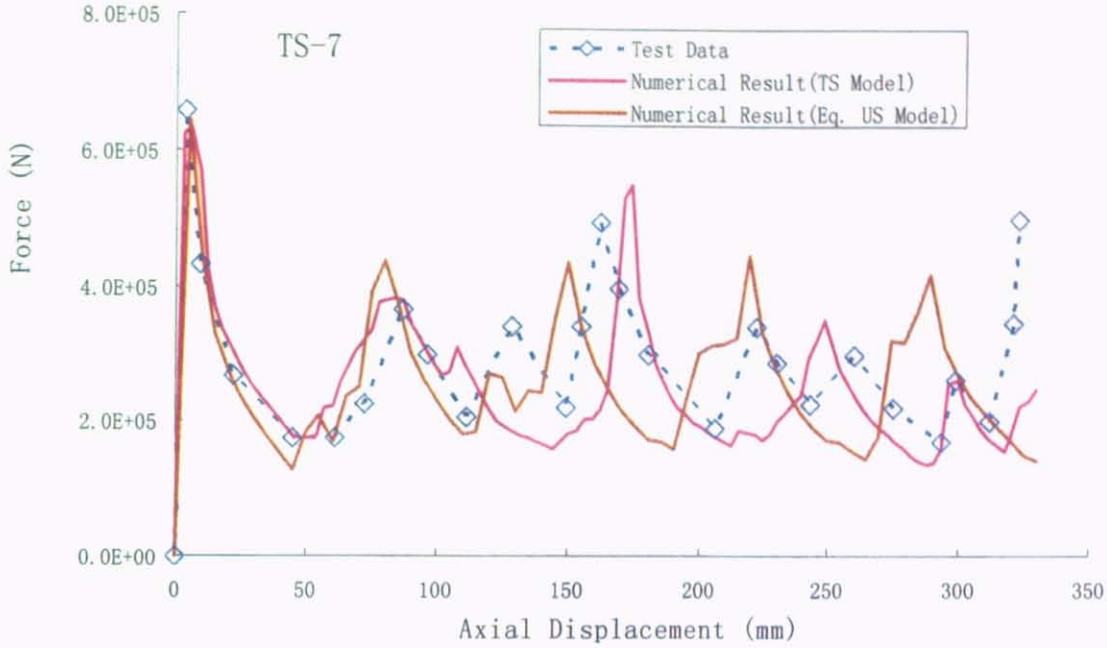

Fig. 3.9 Crushing force curve of transversely stiffened square tube

Table 3.6 Numerical results for transversely stiffened square tube

	P_u (kN)	P_m (kN)
Experimental results	661.5	268.42
Numerical results (Transversely Stiffened Tube Model)	633.27	261.74
Numerical results (Equivalent US Model, 4.3mm)	644.28	263.60

Referring to equation (3.1), the new equivalent plate thickness formula for transversely stiffened square tube which has relatively light stiffeners is given as follows:

$$t_{eq} = t + k_t \frac{A_t}{4b} \qquad 0.028 \le \frac{t_{eq}}{b} \le 0.043 \qquad (3.12)$$

Where: k_t the coefficient accounting for the influence of transverse stiffener

$A_t = N_T \times T_{ST} \times H_{ST}$ the sectional area of transverse stiffeners

As observed from the test results, when the number of the transverse stiffeners increases, the mean crushing strength tends to increase but its effect is small. The transverse stiffeners can also be smeared into the parent plate. The transversely stiffened square tube is replaced by an unstiffened square tube with the equivalent plate thickness calculated from equation

(3.12). Where k_t is an empirical constant accounting for the influence due to the transverse stiffeners. In this study, Based on the equivalent plate thickness data determined by FEM simulation result, the coefficient $k_t = 0.112$ can be obtained by least square method.

Table 3.7 Equivalence plate thicknesses for transversely stiffened square tube

Specimen No.	P_m (kN) (Test data)	$\frac{t_{eq}^{fem}}{b}$	t_{eq}^{fem} (mm) (FEM results)	t_{eq} (mm) (with Eq.(3.12))
TS-1	105.56	0.0281	2.81	2.86
TS-2	118.83	0.0294	2.94	2.89
TS-3	110.39	0.0286	2.86	2.93
TS-4	116.77	0.0292	2.92	2.92
TS-5	132.50	0.0307	3.07	2.99
TS-6	127.98	0.0303	3.03	3.05
TS-7	268.42	0.0430	4.30	4.29
TS-8	294.42	0.0463	4.63	4.39

3.2.4 Numerical Analysis of Orthogonally Stiffened Square Tube

The test specimen OS-13 is selected for numerical modeling and comparison. Fig. 3.10 and Fig. 3.11 show the progressive collapse and the crushing force curve of orthogonally stiffened square tube. Table 3.8 shows the comparison of the experimental results, the numerical results with orthogonally stiffened tube model and equivalent unstiffened tube model.

Table 3.8 Numerical results for orthogonally stiffened square tube

	P_u (kN)	P_m (kN)
Experimental results	454.23	150.23
Numerical results (Orthogonally Stiffened Tube Model)	427.74	147.51
Numerical results (Equivalent US Model, 3.4mm)	424.87	151.58

There are six test specimens for the orthogonally stiffened square tubes. Based on the experimental results and compared with Fig. 3.5, a series of the equivalent plate thicknesses are determined respectively. Table 3.9 shows the equivalent plate thicknesses of orthogonally stiffened square tubes which have relatively light stiffeners.

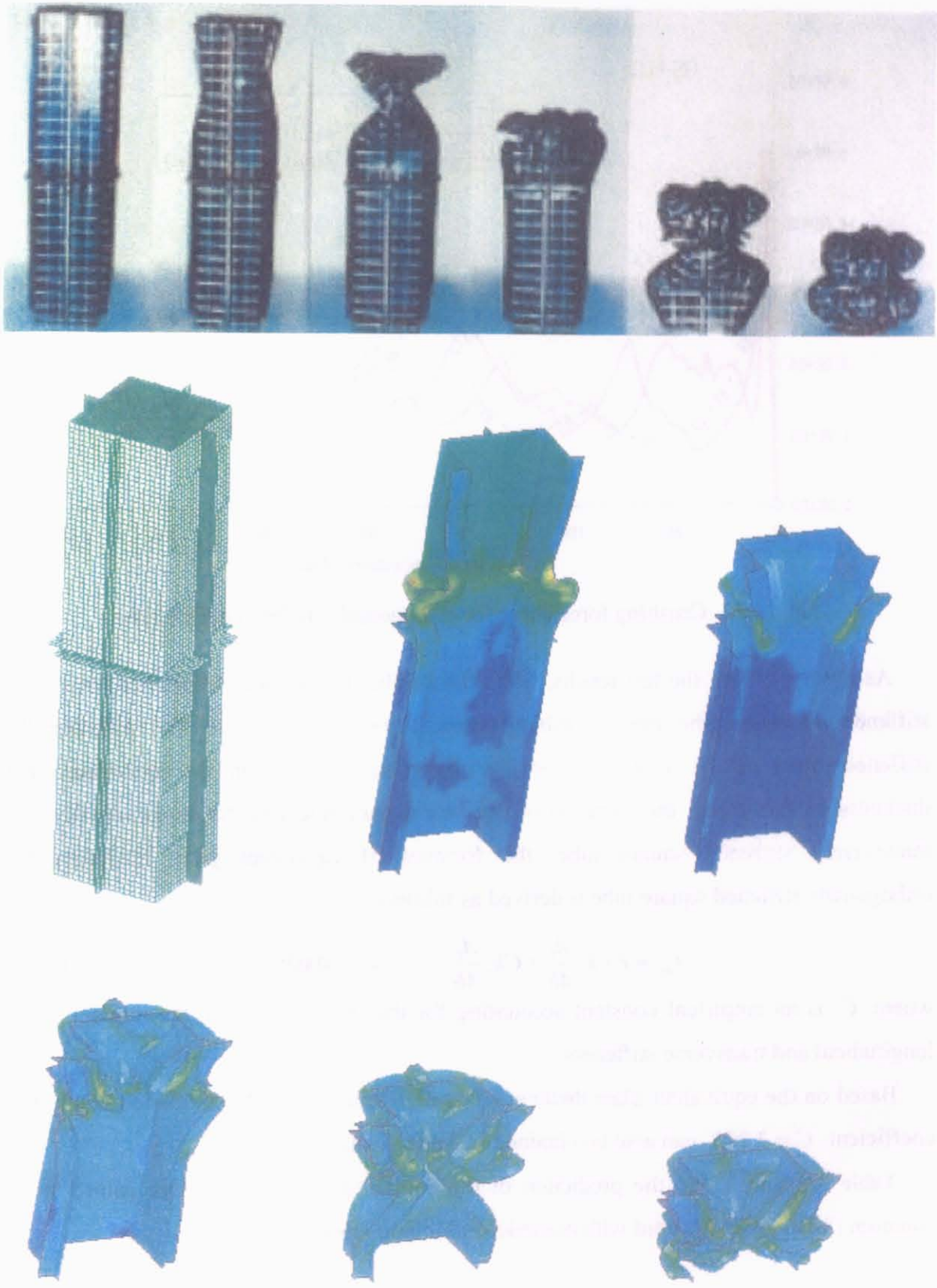

Fig. 3.10 Progressive collapse comparison for orthogonally stiffened square tube

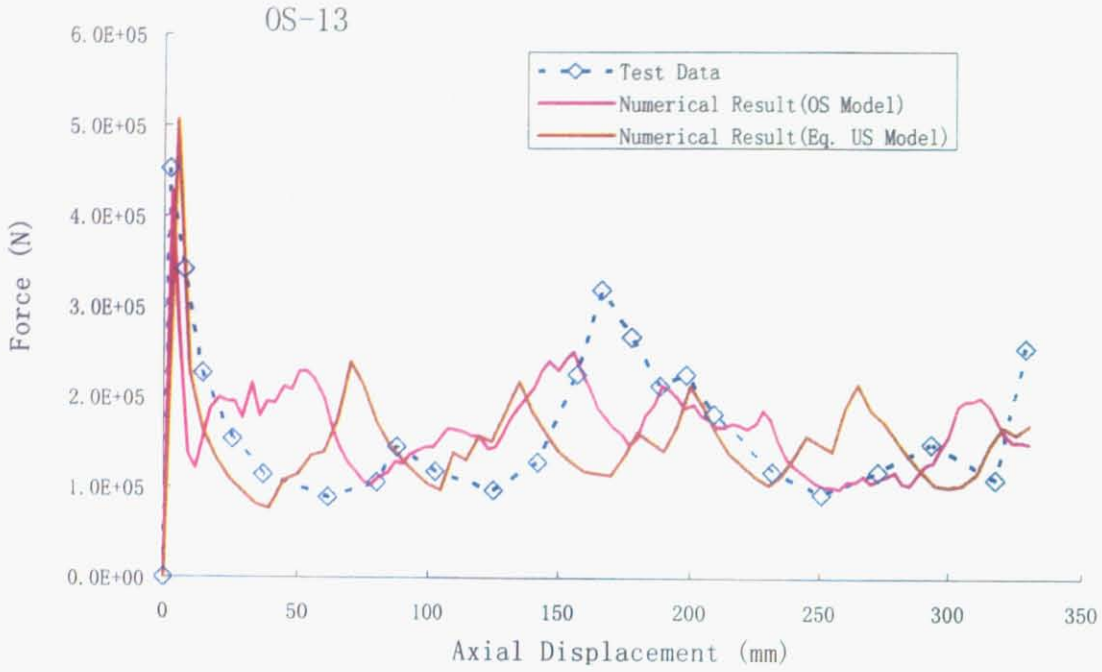

Fig. 3.11 Crushing force curve for orthogonally stiffened square tube

As observed from the test results, when the number of the longitudinal and transverse stiffeners increases, the mean crushing strength tends to increase. The orthogonally stiffened square tube is replaced by an unstiffened square tube with the equivalent plate thickness. In this study, the formulas of equivalent plate thickness for longitudinally and transversely stiffened square tube, the formula of equivalent plate thickness for orthogonally stiffened square tube is derived as follows:

$$t_{eq} = t + k_l \frac{A_l}{4b} + Ck_t \frac{A_t}{4b} \qquad 0.028 \le \frac{t_{eq}}{b} \le 0.043 \qquad (3.13)$$

where C is an empirical constant accounting for the influence due to the interaction of longitudinal and transverse stiffeners.

Based on the equivalent plate thickness data determined by FEM simulation result, the coefficient $C = 3.243$ can also be obtained by least square method.

Table 3.9 shows that the prediction of the equivalent plate thicknesses gained from equation (3.13) are coincident with numerical simulation results

Table 3.9 Equivalence plate thickness for orthogonally stiffened square tube

Specimen No.	P_m (kN) (Test data)	$\frac{t_{eq}^{fem}}{b}$	t_{eq}^{fem} (mm) (FEM results)	t_{eq} (mm) (with Eq.(3.13))
OS-1	185.73	0.0358	3.58	3.59
OS-13	150.23	0.0340	3.40	3.39
OS-14	195.32	0.0367	3.67	3.55
OS-15	201.55	0.0373	3.73	3.83
OS-16	220.62	0.0392	3.92	3.99

3.3 New Formula for the Mean Crushing Load of Square Tube

Because of the finite folding radius, the effective crushing length is always shorter than the original length. Having used the new equivalent plate thickness formulas and the normalized equivalent plate thickness and the ratio of effective crushing length from experiment data are replotted in Fig. 3.12.

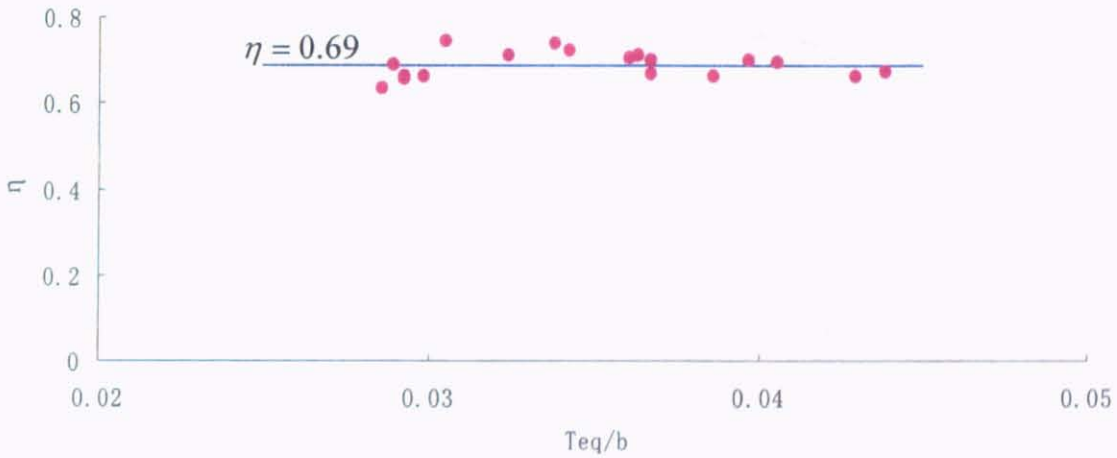

Fig. 3.12 Ratio of effective crushing length

It is observed from Fig. 3.12 that the ratio of effective crushing length is nearly constant regardless of equivalent plate thickness. Here, the ratio of effective crushing length is set as

$$\eta = 0.69 \qquad 0.028 \le \frac{t_{eq}}{b} \le 0.043 \qquad (3.14)$$

Having used the new equivalent plate thickness formulas and normalized the equivalent plate thickness, ultimate load and the mean crushing load, Fig. 3.13 shows the

distribution of the rehandled experimental data. It is very interesting that the distribution of experimental data is nearly linear. So new mean crushing load and the ultimate load can be derived as follows:

$$\frac{P_m}{\sigma_0 A} = \frac{1}{\eta}\left\{7.57\times\left(\frac{t_{eq}}{b}\right)+0.016\right\} \qquad 0.028 \le \frac{t_{eq}}{b} \le 0.043 \qquad (3.15)$$

$$\frac{P_u}{\sigma_0 A} = 10.55\times\left(\frac{t_{eq}}{b}\right)+0.675 \qquad 0.028 \le \frac{t_{eq}}{b} \le 0.043 \qquad (3.16)$$

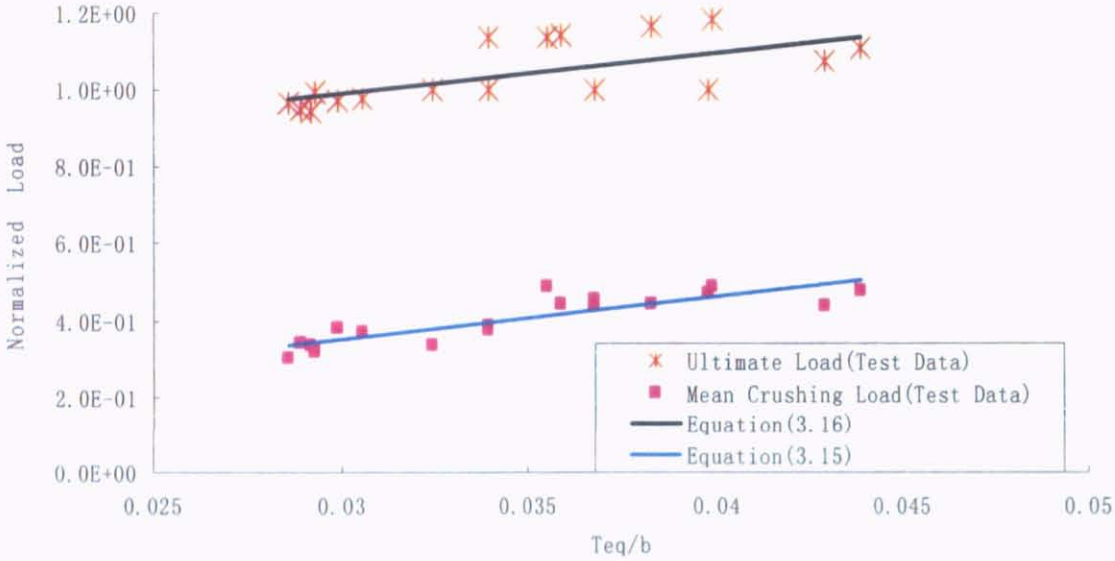

Fig. 3.13 Comparison of new empirical formula with experimental data

Fig. 3.13 shows that new equivalent plate thickness formula, which takes into account the influence of stiffeners in detail, is better than equation (3.1). Table 3.10 and 3.11 show that the result obtained by new mean crushing load formula is coincident with the experimental data and FEM simulation results. Table 3.12 shows that the result obtained by new ultimate load formula also compare well with the experimental data.

For square tube, the situation of each panel is the same in principle and unloaded edges will be very similar to those in a continuous structure. The mean crushing strength of a single plate will be obtained by dividing the total mean crushing strength for the whole tube by a contribution of the four same plates. In the following section, comparison of results obtained by the derived new formulas and existing bow crushing experimental results are carried out.

Table 3.10 Comparison of mean crushing load formulas with experimental data

Specimen No.	Test Results	Jones(1990)		Paik(1996)		Equation (3.15)	
	P_m (kN)	P_m (kN)	Error(%)	P_m (kN)	Error(%)	P_m (kN)	Error(%)
LS-1	161.66	195.18	20.73%	154.55	4.40%	159.2596	1.48%
LS-2	201.08	223.03	10.92%	174.51	13.21%	186.2646	7.37%
LS-4	229.74	252.35	9.84%	195.28	15.00%	215.8926	6.03%
LS-7	133.87	181.81	35.81%	144.89	8.23%	146.3399	9.31%
LS-8	206.16	223.03	8.18%	174.51	15.35%	186.2646	9.65%
TS-1	105.56	144.03	36.44%	117.23	11.06%	113.4093	7.44%
TS-2	118.83	144.03	21.21%	117.23	1.35%	114.5022	3.64%
TS-3	110.39	144.03	30.47%	117.23	6.20%	115.9593	5.05%
TS-4	116.77	144.03	23.35%	117.23	0.39%	115.595	1.01%
TS-5	132.50	144.03	8.70%	117.23	11.52%	118.145	10.83%
TS-6	127.98	144.03	12.54%	117.23	8.40%	120.3307	5.98%
TS-7	268.42	334.12	24.48%	255.91	4.66%	292.9828	9.15%
TS-8	294.42	334.12	13.48%	255.91	13.08%	299.4316	1.70%
OS-1	185.73	195.18	5.09%	154.55	16.79%	168.0023	9.54%
OS-13	150.23	181.81	21.02%	144.89	3.55%	152.6237	1.59%
OS-14	195.32	181.81	6.92%	144.89	25.82%	159.3265	18.43%
OS-15	201.55	223.03	10.66%	174.5	13.42%	193.3681	4.06%
OS-16	220.62	223.03	1.09%	174.5	20.90%	200.9452	8.92%
Mean			16.72%		10.74%		6.73%

Table 3.11 Comparison of mean crushing load formulas with FEM results

Specimen No.	FEM results	Jones(1990)		Paik(1996)		Equation (3.15)	
	P_m (kN)	P_m (kN)	Error(%)	P_m (kN)	Error(%)	P_m (kN)	Error(%)
LS-1	170.44	195.18	14.52%	154.55	9.32%	159.26	6.56%
LS-2	199.61	223.03	11.73%	174.51	12.58%	186.26	6.69%
LS-4	210.06	252.35	20.13%	195.28	7.04%	215.89	2.78%
LS-7	134.70	181.81	34.97%	144.89	7.57%	146.34	8.64%
LS-8	185.83	223.03	20.02%	174.51	6.09%	186.26	0.23%
TS-1	105.84	144.03	36.08%	117.23	10.76%	113.41	7.15%
TS-2	113.36	144.03	27.06%	117.23	3.41%	114.50	1.01%
TS-3	107.98	144.03	33.39%	117.23	8.57%	115.96	7.39%
TS-4	116.30	144.03	23.84%	117.23	0.80%	115.60	0.61%
TS-5	131.86	144.03	9.23%	117.23	11.10%	118.15	10.40%
TS-6	134.79	144.03	6.86%	117.23	13.03%	120.33	10.73%
TS-7	261.74	334.12	27.65%	255.91	2.23%	292.98	11.94%
TS-8	308.04	334.12	8.47%	255.91	16.92%	299.43	2.79%
OS-1	176.37	195.18	10.67%	154.55	12.37%	168.00	4.74%
OS-13	147.51	181.81	23.25%	144.89	1.78%	152.62	3.47%
OS-14	177.33	181.81	2.53%	144.89	18.29%	159.33	10.15%
OS-15	210.92	223.03	5.74%	174.5	17.27%	193.37	8.32%
OS-16	220.24	223.03	1.27%	174.5	20.77%	200.95	8.76%
Mean			17.63%		9.99%		6.24%

Table 3.12 Comparison of new ultimate load formula with experimental data

Specimen No.	Pu (kN) (Test results)	Pu (kN) (Equation (3.16))	Error(%)
LS-1	417.66	431.36	3.28%
LS-2	452.46	481.15	6.34%
LS-4	487.27	533.59	9.51%
LS-7	400.27	407.06	1.70%
LS-8	452.65	481.15	6.30%
TS-1	337.12	340.01	0.86%
TS-2	331.24	341.11	2.98%
TS-3	346.92	342.58	1.25%
TS-4	329.28	342.21	3.93%
TS-5	338.59	344.78	1.83%
TS-6	340.55	346.99	1.89%
TS-7	661.5	694.86	5.04%
TS-8	685.02	701.36	2.39%
OS-1	476.77	440.18	7.68%
OS-13	454.23	413.39	8.99%
OS-14	454.72	420.15	7.60%
OS-15	527.24	488.31	7.38%
OS-16	535.57	495.95	7.40%
Mean			4.80%

3.4 Application to Bow Crushing Model Test

In this section, comparison of results obtained by the derived new formula and existing bow crushing experimental results are carried out.

Amdahl (1983) performed a series of model tests of bow crushing. A wedge-shaped bow including longitudinal stiffeners on the side shell model specimens is chosen here for comparison. The main dimensions and structural arrangements of the test model are shown in Fig. 3.14. The model is made of 3.0 mm thick mild steel plates. Frames and stiffeners are made of 3.0 mm flat bars. The average flow stress of the material is 350 MPa. The bow model is crushed progressively during the tests. The crushing process has divided into two stages

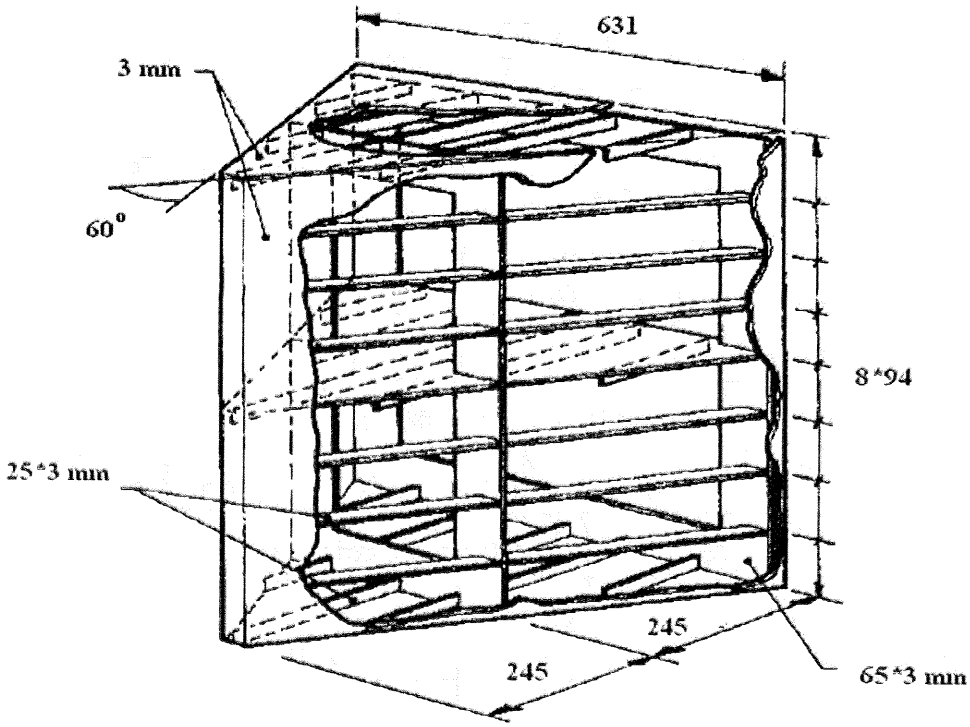

Fig. 3.14 Wedge-shaped bow model test by Amdahl(1983)

Table 3.13 Material property for bow model

	Thickness (mm)	Elastic Modulus (GPa)	Yield Strength (MPa)	Ultimate Stress (MPa)
Plate	3.0	206	310	390
Stiffener	3.0	206	310	390

■ Stage 1 (till the deck and side plate touch the first frame, $\delta_{max} = 169\ mm$)

Table 3.14 Mean crushing load and ultimate load for bow model at stage 1

	b (mm)	Present Method			
		t_{eq} (mm)	t_{eq}/b	P_u (KN)	P_m (KN)
Deck plate	206	3.624	0.0176	315.4	195.7
Side plate	376	3.628	0.0097	710.4	213.5
Bow model				1025.8	409.2
Test data				1003.3	533.5

■ Stage 2 (till the deck and side plate touch the second frame, $\delta_{max} = 338\ mm$)

Table 3.15 Mean crushing load for bow model at stage 2

	b (mm)	Present Method		
		t_{eq} (mm)	t_{eq}/b	P_m (KN)
Deck plate	489	3.624	0.0074	224.6
Side plate	376	3.628	0.0097	213.5
Bow model				438.1
Test data				533.5

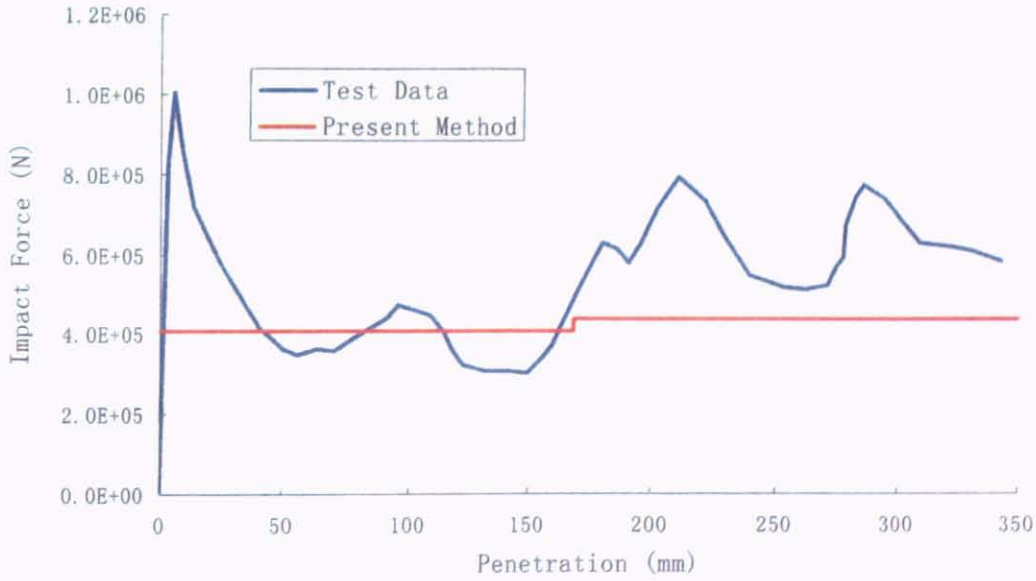

Fig. 3.15 Comparison between predication and test data for bow model experiment by Amdahl(1983)

The proposed new mean crushing load and ultimate load formulas are checked against existing bow model test. In summary, the comparison of crushing load and ultimate load obtained by new formulas (Eqs. 3.15 and 3.16) and test data are shown in Fig. 3.15, Table 3.13 and Table 3.14. It is clear that new formulas give good prediction of mean crushing load and ultimate load for bow structures. It is also illustrated that the proposed formula can be used in practical applications well.

3.5 Remarks

The crushing collapse of thin-walled structure components is one of the important failure modes during ship collision and grounding. In order to improve the structural crashworthiness in collision and grounding, it is necessary to better understand the mechanics of ship collision and grounding such as crushing collapse of thin-walled structure components. For relatively light stiffeners, experimental data of stiffened square tube showed that the effect of the transversely stiffeners on the mean crushing load is significant, which was often neglected in previous simplified analytical approach. Based on these test results, the longitudinally stiffened square tube, transversely stiffened square tube and orthogonally stiffened square tube can be reasonably replaced by an unstiffened squre tube with the equivalent plate thickness. Since nonlinear finite element model simulations provide much detailed information than simplified analytical approaches, benchmark studies on simplified analytical method, nonlinear FEM and experimental results for axial crushing of thin-walled structure are carried out in this chapter. By comparing the experimental data with FEM simulation results, the new equivalent plate thickness formulas for the longitudinally stiffened square tube, transversely stiffened square tube and orthogonally stiffened square tube are derived, respectively. The predicting results of the new mean crushing load formulas and ultimate load formula are in fair agreement with the experiment data when the application condition $0.028 \leq \frac{t_{eq}}{b} \leq 0.045$ is satisfied. It is also illustrated that the proposed formulas can be used well in practical applications such as prediction of the load-carrying capacity for bow crushing.